Advanced Deployable Shell-Based Composite Booms For Small Satellite Structural Applications Including Solar Sails

By Juan M. FERNANDEZ[1)]

[1)] *NASA Langley Research Center, Structural Dynamics Branch, Hampton, VA 23681, USA.*
juan.m.fernandez@nasa.gov

The long list of advantages that small satellites can offer in terms of fast development time, low cost, possibility of large swarm missions, scientific and/or educational return on investment are, in general, in conflict with the challenging mass and volume constraints imposed on the spacecraft subsystems. Many systems such as solar panels, antennas, sensors, telescopes, solar sails, drag sails, sun shades, radiators, and payloads are in need of reliable deployment of structural booms and arrays for power generation, communications, propulsion, deorbiting, thermal control and scientific instruments. The paper presents ongoing research and development of thin-shell rollable composite booms designed under the particularly stringent and challenging requirements of CubeSat-based solar sails. Several new boom concepts are proposed and other existing ones are improved upon using thin-ply composite materials to yield unprecedentedly compact deployable structures for a wide range of small satellite applications. Many laminates were investigated on short sections of each boom design, and the most promising ones were selected for the fabrication of longer booms. Inducing bi-stability on some of the booms was studied experimentally by choosing a particularly different laminate construction for each of the two thin-shell walls producing favorable results. For every boom introduced, the scalable fabrication process developed to keep the overall boom system cost down is shown. Finally, the initial test results carried out with purposely designed boom structural characterization test methods with gravity off-loading are presented to compare the structural performance of the booms under expected operational and general load cases.

Key Words: Composite booms, bi-stability, solar sails, small satellite deployable structures, structural characterization.

1. Introduction

With the miniaturization of electronic systems and spacecraft components, the space industry also saw room to develop satellite platforms of a much more reduced size that carry less costs overall. Over the last decade with the birth of CubeSats, the Evolved Expendable Launch Vehicle Secondary Payload Adapter (ESPA) ring and similar small satellite adapters carried aboard launchers, sounding rockets or reusable spacecraft, the access to space has opened up to institutions other than large national space agencies and companies promoting the expansion of small satellite systems. As a result, small satellites of the future may provide comparable or even better performance than much larger satellites of the past. However, for this to happen, much of the functionality of the larger platforms, which was partially achieved with the use of large deployable structures, needs to be transferred to the smaller systems via highly compact and reliable deployable systems with unprecedented packaging efficiencies and areal weights.

High performance state-of-the-art deployable structures are mainly being designed for medium (1-10 m^3) to large (>10 m^3) size satellites. The lack of reliable deployable structural systems for low-cost, small size (< 1 m^3), rideshare-class spacecraft platforms severely constrains the potential for using small satellite platforms on high return on investment missions. There is thus a need for reliable, lightweight, high packaging efficiency deployable booms that can serve as the supporting structure for a wide range of small satellite systems. The National Air and Space Administration (NASA) is currently investing in the development of a new class of advanced deployable composite booms to support future deep space science and exploration precursor missions to be carried out with small spacecraft. The concepts are being designed to: meet the unique requirements of small satellites, maximize ground testability, permit the use of low-cost manufacturing processes that will benefit scalability, be scalable for use as elements of hierarchical structures (e.g., trusses), allow long duration storage, have high deployment reliability, and have controlled deployment behavior and predictable deployed dynamics. This paper will present the various rollable boom concepts that are being developed internally for 5-20 m class size structures using the so called High Strain Composites (HSC) thin-ply materials.[1)] One of the near term applications under study of such composite booms is for deep space solar sails for science, exploration and technology demonstration missions.

2. Reference Application & Boom Requirements

The deployable composite booms to be presented are being developed to expand the portfolio of available rollable booms for small satellites and maximize their length for a given packaged volume. Given that solar sails are a great example of volume and mass optimization, the booms were designed to comply with nominal solar sail requirements on 6U CubeSats, that are a good compromise between those of smaller form factors (1U, 2U and 3U CubeSats) and larger ones (12U and 27 U CubeSats and ESPA-class microsatellites). NASA is also working on the Near Earth Asteroid (NEA) Scout[2)] 6U CubeSat solar sail mission to be launched in 2018-2019 as part of Exploration Mission 1 (EM-1). Hence, the solar sail subsystem requirements for this mission served as a reference scenario for the development of these composite booms.

Some of the solar sail system requirements for the NEA Scout mission applicable to the booms are:

- Deployed highly reflective surface area ≥ 85 m^2.
- Stowed solar sail system volume ≤ 100 mm x 200 mm x 150 mm (3 U).
- Stowed solar sail system mass ≤ 3.5 kg (2.5 kg preferred).
- Average nominal sail membrane stress ≥ 70 kPa.
- Minimum deployed natural frequency ≥ 0.1 Hz.
- Pre-operational life ≥ 1 year in a stored condition.
- Mission life ≥ 3 years in deep space (≤ 2 AU from the Sun) including lunar vicinity.
- Deployed sail surface as flat as possible considering all thermal and mechanical loads and residual stresses.

As these booms are designed with the purpose of advancing the state-of-the-art of rollable booms, such as the Elgiloy Triangular Rollable And Collapsible (TRAC) booms baselined for NEA Scout [3], they should also meet, where possible, the following additional requirements:

- Deployed boom length ≥ 6.85 m.
- Stowed volume for four booms and deployment mechanisms ≤ 100 mm x 200 mm x 60 mm (1.2 U).
- Boom buckling load under realistic boundary conditions ≥ 3 N. This includes a safety factor of two.
- Mass of each boom ≤ 0.25 kg (≤ 0.15 kg preferred), assuming a 1.25 kg (1 kg preferred) boom deployer.
- Stowage creep effect should produce ≤ 30% boom cross-section flattening, and ≤ 10 cm boom axial curvature (out-of-true lateral tip deflection) over pre-operational life of ≥ 1 year.
- Withstand deep space (≤ 2 AU from the Sun) environment (thermal, UH vacuum, radiation) ≥ 3 years.
- Coefficient of thermal expansion in the boom axial direction ≤ 1 E-6 m/m-°C.
- Reduce the strain energy level of the coiled configuration compared to similar metallic booms by a factor of ≥ 2.

Let us assume that we are to develop four 6.85 m booms to fit inside a 1.2 U volume including the deployment mechanisms. This volume requirement can be broken down into several ones assuming that there will be two booms co-coiled on each of the two hubs of 100 mm x 100 mm x 60 mm volume. Considering some peripheral components of the boom deployer necessary to constrain and guide out the booms properly, the effective maximum allowed stowed volume left for each of the two-boom coils is 97 mm x 97 mm x 45 mm, where the 45 mm is the flattened height of the boom, h. The 97 mm^2 footprint area can be translated to an outer radius of the coil, r_f, of 48.5 mm. The first geometric parameter, h, will have a great effect on the boom as it determines the size of the cross-section for a given boom shape. Note that this is equal to the cross-section arc-length for the case of cylindrical and triangular shell-based booms. Whereas the second geometric parameter, r_f, determines the maximum boom thickness, t_b, permitted for a given boom length, L, or in our case the size of the solar sail.

Therefore, for small satellite applications, it is the system volume requirement that is the one that imposes size and thickness constraints on the booms, which directly translate to stiffness and strength limitations that ultimately need to comply with structural requirements. Hence, volume constraints can, from the start, discard thin-walled boom options for a required solar sail size. For example, single-shell Storable Tubular Extendible Member (STEM) booms[4] cannot normally be used for these highly height constrained applications given their large arc-lengths.

The outer radius of the coil, r_f, for a two-boom system can be calculated using the Archimedean spiral approximation as:

$$r_f = r_i + w\, t_t\,, \tag{1}$$

where r_i is the initial coiling radius, which normally is equal to the radius of the drum/spindle, w is the number of total windings or wraps, and t_t is the total thickness of all the co-reeled booms, that can be approximated by:

$$t_t = n\, t_{sh}\,(1 + \mu)\,, \tag{2}$$

where n is the total number of thin-shell walls coiled, t_{sh} is the thickness of the thin-shell wall, and μ is the packaging efficiency parameter that adds a percentage of the thin-shell thickness.

The total number of wraps of the coil, w, can be calculated from:

$$w = \sqrt{\left(\frac{r_i}{t_t}\right)^2 + \frac{L}{\pi\, t_t}} - \frac{r_i}{t_t}, \tag{3}$$

where L is the length of each boom co-wrapped.

Fig. 1. (a) shows the outer coiling diameter (OD) of two co-reeled booms, $2\, r_f$, of length $L = 6.85\ m$ (for a 85 m^2 sail) plotted against the shell thickness, t_{sh}, for two initial coiling diameters (ID), $2\, r_i$. For this case (two booms), the number of thin-wall sections can either be $n = 2$ for one-wall booms (STEMs [4] and tape-springs [5-7]) or $n = 4$ for two-wall booms (lenticular () shaped booms [8], TRACs [9] and Collapsible Tubular Masts (CTMs) [10]). The packaging efficiency parameter was set to $\mu = 0.25$ (25% of t_{sh}) following empirical data. It can be seen that the 97 mm outer diameter constraint translates to a maximum permitted total boom thickness, $t_b = t_t/n$, for two-wall booms of 0.37 mm and 0.32 mm for initial coiling diameters of $2\, r_i = 45\ mm$ and $2\, r_i = 55\ mm$, respectively. As expected, it is concluded that the smaller the initial diameter of the coil, the thicker and thus stiffer the booms can be made.

However, the minimum initial coiling diameter, $2\, r_i$, for a given section thickness, t, is normally determined by the material maximum strain to yield in the boom axial direction, ε_{y11}, which can be approximated by Eq. 4 considering Euler-Bernoulli beam theory of a thin-walled section:

$$\varepsilon_{y11} = \frac{E_{11}}{\sigma_{y11}} = \frac{t}{2\,r_i}, \tag{4}$$

where E_{11} is the material Modulus of Elasticity in the boom axial direction and σ_{y11} is the maximum stress for elastic coiling or yield stress in the boom axial direction. Note that $t = t_b$ for joined-shell booms and $t = t_{sh}$ for separate-shell booms.

From Fig. 1. (b) it is clear that the worst case occurs for joined-shell boom designs that are initially coiled about small diameter drums. Hence, structures like the TRAC and CTM booms would need to be ultra-thin to fit within CubeSat volumes or be reeled onto significant size drums hindering their scalability.

Eq. 4 can also be used to define the maximum curvature ($1/r_{sh}$) that any segment of the boom cross-section should have, as this needs to be flattened prior to being coiled around the drum. For this, the appropriate axis to consider is aligned with the boom transverse/hoop direction. Transverse properties are defined here by the $_{22}$ subscript. Thus, Eq. 4 translates to:

$$\varepsilon_{y22} = \frac{E_{22}}{\sigma_{y22}} = \frac{t_{sh}}{2\,r_{sh}}, \tag{5}$$

where r_{sh} is the radius of a shell segment of the boom cross-section.

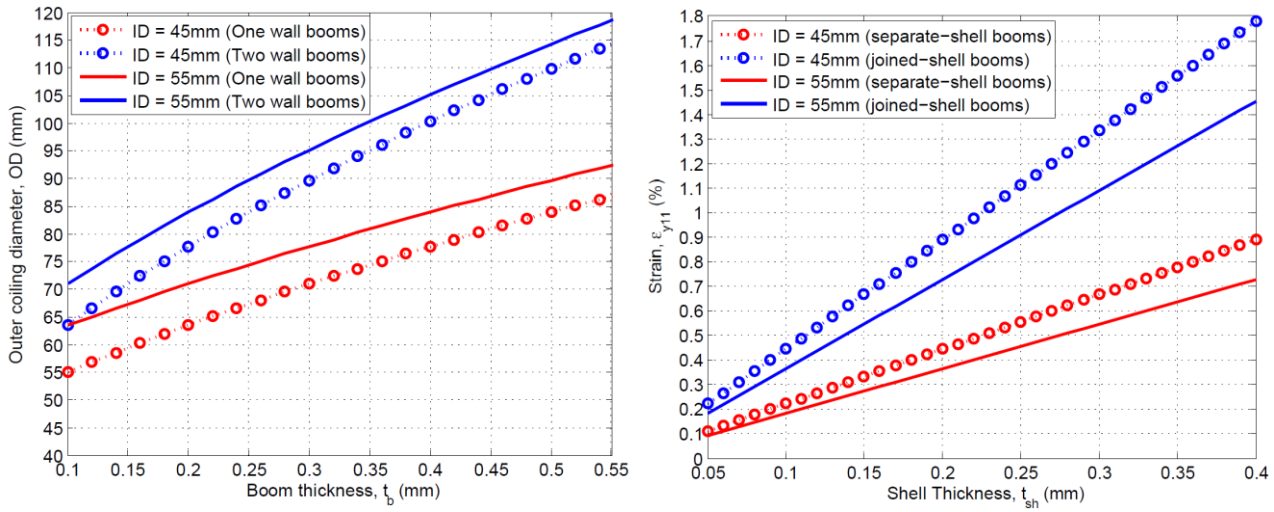

(a) (b)

Fig. 1. (a) Outer coiling diameter versus boom thickness for different initial coiling diameters and number of wall sections per boom. Here two 6.85 m long booms are co-reeled; (b) strain versus thin-wall shell thickness for different initial coiling diameters and types of shell structures.

As far as the mass requirement is concerned, for a boom length of 6.85 m, this translates to a boom linear density requirement of $LD \leq 36.5$ g/m (≤ 21.8 g/m preferred). Also, considering a two-wall boom design with a flattened height of $h = 45$ *mm*, the maximum total areal weight for both thin-shell composite walls including the weight of any possible bonding adhesive is $AW = LD/h \leq 810$ *g/m*^{2} (≤ 484 *g/m*^{2} preferred). For symmetrical boom designs, the maximum areal weight of each thin-shell wall would obviously be half of these values. Now, considering carbon fiber as the baseline lightweight material for the booms, which has an average density of $\rho = 1570$ *kg/m*^{3} when used in combination with epoxy resins (60% fiber volume fraction, *FVF*), this ultimately translates to a maximum total boom structural thickness requirement of $t_b = AW/\rho \leq 0.52$ *mm* (≤ 0.31 *mm* preferred). Note that the thickness of any possible adhesive used would be added on top of the structural thickness. The total boom thickness requirements derived from mass and volume requirements then needs to be compared to assess which is the critical one.

3. Thin-Ply Materials

As seen, for a given boom length and flattened height constraint, the thickness and material selection is critical to meet mission volume, mass and structural requirements. To be able to comply with stringent thickness and areal weight requirements, the new so-called thin-ply composites are the preferred materials of choice. The use of thin-ply composites is one area of composites technology that has not yet been fully explored or exploited by NASA. Thin-ply composites are those with cured ply thicknesses (CPT) below 0.065 mm for unidirectional (UD) materials and double that for textile fabrics. By comparison, a standard-ply-thickness UD material would have a CPT of approximately 0.125 mm. Commercially-available prepregs and dry fabrics are now available with ply thicknesses as thin as 0.018 mm for UD materials and 0.055 mm for weaved fabrics. The ever growing material and product developments surely open up the design space for the laminates of rollable composite booms. In addition, thin-ply composites hold potential for reducing structural mass and increasing performance when compared to standard-ply-thickness laminates in terms of: resistance to micro cracking, resistance to delamination, improved damage tolerance, improved aging and fatigue resistance, reduced minimum-gage thickness and increased scalability.

Common early failure modes of rollable booms subjected to high strains are resin micro cracking and ply delamination that severely limit the full utilization of the fiber strength. Micro cracking normally onsets at strains of just 0.5 % [5], well below the intended operational strain of HSC booms. Hence, if this failure mode can be suppressed by design, composite laminates could

carry loads up to the failure strain limits of most modern carbon fibers, which is about 2 % in tension and 1 - 1.5 % in compression.

The down side of using thin-ply materials is: their difficulty to acquire (high cost, long lead times and low availability, particularly on high modulus fibers that are more difficult to spread), lower quality (some degree of fiber twisting, misalignment and damage, thickness non-uniformity and gaps in the material), difficulty to obtain in rolls more than 35-40 mm wide without joining them (affects fiber misalignment), and almost no aerospace qualification process carried out on them. In particular, the extremely low weight forms are fabricated on a best effort-basis.

To fabricate the booms proposed herein, the thin-ply materials shown in Table 1 were purchased. The carbon fiber materials are some of the lightest intermediate modulus (IM) products available worldwide to date with resins that have space heritage. The S-2 glass and Astroquartz products were also sourced in their lightest form available. Note that the values presented are the areal weight (AW) of the lamina/ply at 60% FVF and not the fiber areal weight (FAW) that is normally used to source the dry fabrics. Most of the materials purchased are spread-tow fabrics that are fabricated from large tow (12-24K) unidirectional fiber bundles that go through a cumbersome spreading process to reduce their thickness by up to six fold. All the laminates investigated combine these materials to achieve high performance booms that maximize stiffness (EI), mass and volume.

Material (fiber / resin)	Form	Lamina AW (g/m2)	Measured Cured Ply Thickness (mm)	E_{11} (GPa)	$\varepsilon_{11u,\,C}$ (%)	Vendor (fiber / resin)
MR60H / PMT-F7 (CF)	UD SpT	56	0.040 ± 0.05	174.3	1.10	Oxeon / Patz M&T
IM7 / RS-36 (CF)	UD SpT	44	0.032 ± 0.05	166.0	1.06	Tencate / Tencate
HTA40 / PMT-F7 (CF)	PW SpT	90	0.075 ± 0.01	75.9	1.03	TCS / Patz M&T
T300-1K /PMT-F7 (CF)	BR	125	0.100 ± 0.01	73.8	1.06	A&P / Patz M&T
AstroQuartz II/PMT-F7	PW (525)	93	0.080 ± 0.01	25.6	2.24	JPS Comp /Patz M&T
S2-Glass / PMT-F7	UD SpT	100	0.055 ± 0.05	57.2	2.56	Patz M&T/Patz M&T

Table 1: Thin-ply materials and properties used for research and development of the composite booms. The properties presented are for laminae where the fibers are aligned with the boom axial direction (0° or $_{11}$) and using the rule of mixture for a 60% fiber volume fraction (FVF). The compressive failure strain, $\varepsilon_{11u,\,C,}$ is much lower than the tensile or bending failure strain but is listed here as a lower bound failure case.
CF – carbon fiber; UD – unidirectional; PW – plain weave; BR – braid; SpT – Spread-tow.

4. Mini-CTM or Omega Boom

Given its superior structural performance capabilities, the closed-section tubular masts with joined seams has been the rollable boom more investigated since its inception in the United States in the 1960s.[11] The first notable use in space for this boom type was to collect soil samples on Mars during the Viking 1 and 2 missions in 1976.[12] These so-called Collapsible Tubular Masts (CTM) were made from thin metal sheet, aside from some early investigations in the late 1970s to fabricate them in carbon fiber reinforced plastic (CFRP).[13] The first CFRP CTM booms were developed by Sener in Spain in the mid-1980s under the European Space Agency (ESA) umbrella.[14] ESA spent significant funds developing a continuous manufacturing method for these CTM booms in view of creating very large structures.[15] In the late 1990's, DLR rekindled the boom concept for solar sail applications using more modern composite materials and analysis software packages.[10] Since then, both scaled up [16] and scaled down [17] versions of the early booms have been developed by DLR, although none of them have yet been able to prove their worth in space. The current NASA investigation shown herein aimed to develop the smallest CTM composite booms to date, of just 45 mm in flattened height, in order to comply with the aforementioned requirements of CubeSat-based deep space solar sail missions.

Boom designers face conflicting requirements of the stowed and deployed configurations. For the former, it is desired to have a laminate design with a high strain to yield/failure, ε_y, for compact stowage and aid towards creep reduction, as well as a low axial Young's modulus, E_{11}, to have a less energetic system while stowed and during deployment. For the latter, it is desired to have a high axial modulus for boom stiffness (EI) maximization, as in slender boom structures, the failure modes, global column or local wall buckling, are both determined by stiffness rather than material strength. This is normally realized by maximizing the percentage of fibers running parallel to the axis of the boom. From a cross-section geometry standpoint, in general, it is desired to have a small radius of curvature in the cross-section to maximize the moment of area but at the expense of an increase in flattening stresses and strains that tend to pose a limit on the design space.

To assist in the trade-off process, an initial parametric analysis was run in Matlab with system requirements acting as constraints to determine the optimal boom cross-section geometry that maximized the moments of area about the principal axes, I_{xx} and $I_{yy,}$ and the torsional constant, J, while keeping the flattening strains, ε_{22}, and rolling strains, ε_{11}, within acceptable levels. The validated engineering equations from 18) were used to calculate the mechanical properties of the booms and their state of stress, strain and strain energy in the coiled configuration. These formulas provide a good initial guess for iterations required during critical design. A visualization tool was also developed to view the geometries generated and create meshes for finite element modeling (FEM).

The following design parameters were used in the trade analysis:

- The cross-section geometry was defined by joining three equal circular segments, in the shape of the Greek letter omega, Ω, on two flat regions at each end, called the web. See Fig. 2 for reference. These equal curvature arcs subtend

an angle of $50^{o} \leq \alpha \leq 90^{o}$. Parabolic segments or dissimilar arcs are not sought after as the small flattened height with which to work would have prevented their benefits.

- The width of the web was $3\ mm \leq \omega \leq 5\ mm$. Smaller widths will result in unwanted large shear stresses at the bonded edges and larger widths depart from the optimal design.
- The materials from Table 1 were used to create a range of possible laminates even though silicon-based materials were bounded to produce less stiff designs. Combinations of them in lay-ups of the following form were assessed: $[45PW/0_n]$, $[0\text{-}90PW/0_n/]$, $[0\text{-}90PW]_n$, and $[45PW]_n$, where $n = 1,2$. The outer surface plies considered had only plain weave (PW) laminae as it is known that axial unidirectional surface plies tend to delaminate prematurely at high strains. Thus, the wall thickness at each boom half, t_{sh}, and the total thickness at the web, t_b, varied accordingly.

The following geometric constraints and mission requirements were used in the parametric analysis:

- Flattened height of $h = 45\ mm$.
- Maximum outer diameter of the coil of $2\ r_f = 97\ mm$, for two co-reeled booms of $L = 6.85\ m$.
- Initial coiling diameter was set at $2\ r_f = 45\ mm$.
- Given a thickness of the adhesive of 0.09 mm, the maximum shell thickness was set at $t_{sh} = 0.14mm$, in order to comply with packaging requirements.
- Symmetrical boom construction, i.e. both thin-wall shells have the same laminate.
- Given an areal weight of the adhesive of 145 g/m^2, the maximum areal weight for each thin-shell wall was set at $AW = 220\ g/m^2$, in order to comply with the preferred mass requirement.
- Maximum boom laminate axial coefficient of thermal expansion (CTE) of $\alpha_{CTE,11} = 1\ ppm/°C$.
- Maximum strains in both principal directions of $\varepsilon_{11,22} = 0.8\%$.
- Maximum boom Euler buckling load of $P_{cr} = 3\ N$ for a boundary condition halfway between fixed-free and pinned-pinned, in accordance with previous analytical models of four-quadrant solar sails.[19-21] This translates to a minimum bending stiffness requirement of $E_{11}I_{xx,yy} = 20.2\ Nm^2$ in both principal boom axes x and y.

It was determined that a two-ply [45PW/0] lay-up, with the HTA40 / MR60H spread-tow carbon materials, respectively, was the optimal laminate for the Mini-CTM or Omega booms. The maximum shell thickness requirement discarded laminates with more than two plies, and the thicker MR60H unidirectional material maximized boom axial stiffness and resistance to creep while complying with all of the packaging requirements. Each thin-shell is theoretically only 0.115 ± 0.015 mm thick, which provides some margin for loss of packaging efficiency and an increase in total boom thickness due to non-uniformity in the bond line thickness and outer surface roughness (resin build-up) due to breather material imprint. The outer surface ±45° bias plies (45PW) are only as thick as needed for cross-section stability and torsional stiffness. It has been previously shown that surface biased plies add shear stiffness and local bending stiffness, that supresses the typical fiber compressive micro-buckling failures modes of the highly loaded inner axial (0°) plies, while also prevents surface cracking during packaging.[1] Note that this laminate is non-symmetrical in every section of the boom other than the bonded edges where the resulting laminate is symmetrical $[45PW/0]_s$. This has a negative effect during fabrication as thermal stresses tend to promote an axial curvature in the final boom, although this deformation has been well managed as will be shown. The computed axial modulus of this laminate is $E_{11} = 71.7\ GPa$, and it has a near zero theoretical axial CTE for optimal boom thermal performance of $\alpha_{CTE,11} = -0.07$ ppm/°C.

Fig. 2. shows the coordinate axis adopted, as well as the design parameters that represent the cross-section of the booms: subtended angle, α, shell section radius, r_{sh}, shell section thickness, t_{sh}, and web section width, w.

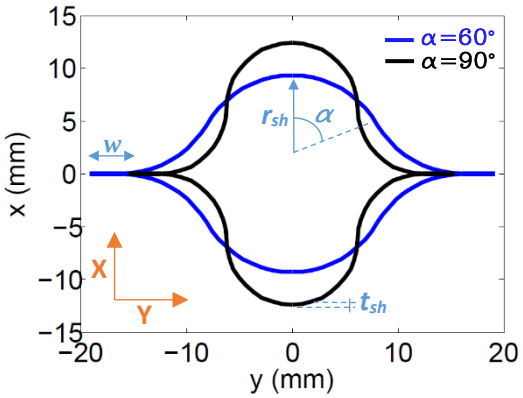

Fig. 2. X-Y plot of two Omega boom cross-sections of subtended angles $\alpha = 60°$ and $\alpha = 90°$.

Fig. 3 shows the acceptable design space that complies with bending stiffness requirements for the [45PW/0] laminate aforementioned. It can be seen that the out-of-plane stiffness of the boom, represented by I_{xx}/t_{sh}, is acceptable for all design combinations. However, the weaker axis of the booms, x, restricts the design space. Booms of a subtended angle below 58° and 72° for a web width of 3 mm and 5 mm, respectively, will not have sufficient in-plane bending stiffness, represented by I_{yy}/t_{sh}. This is of special concern as it is known that flattening of the cross-section (decrease of subtended angle) will develop over long periods of stowage due to material creep, and therefore a deformed boom may not perform as intended during operation.

From the graph of Fig. 3, it is clear that it is desirable to have the largest subtended angle possible with the lowest web width in order to maximize I_{yy}. Unfortunately, this trend will result in a small radius of curvature of the shell section and therefore high strains during flattening. Fig. 4 presents the region of acceptable transverse strain for the laminate of study. It is shown that boom designs with a subtended angle above 80° and 72° for a web width of 3 mm and 5 mm, respectively, will result in flattening strains above 0.8%, which is considered herein to be the maximum acceptable. Designs with a web width of $w = 5$ *mm*, and a subtended angle of $\alpha = 72°$ are thus already at the limit. To account for the flattening of the cross-section over time, it is thus desired to start with the largest possible subtended angle and the smallest web width. Therefore, the final boom design adopted for fabrication of the molds has an as-manufactured subtended angle of $\alpha = 80°$ and a web width of $w = 3$ *mm*.

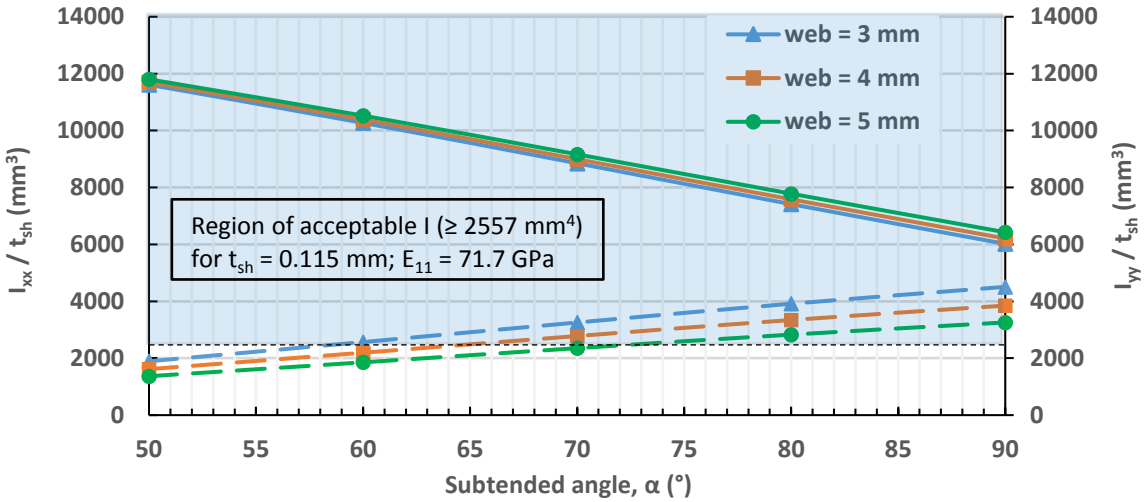

Fig. 3. Moment of area, I, divided by the shell section thickness, t_{sh}, in both principal directions, x and y, for different combinations of the cross-section subtended angle, α, and the web width, w. The solid and dashed lines correspond to I_{xx} and I_{yy}, respectively.

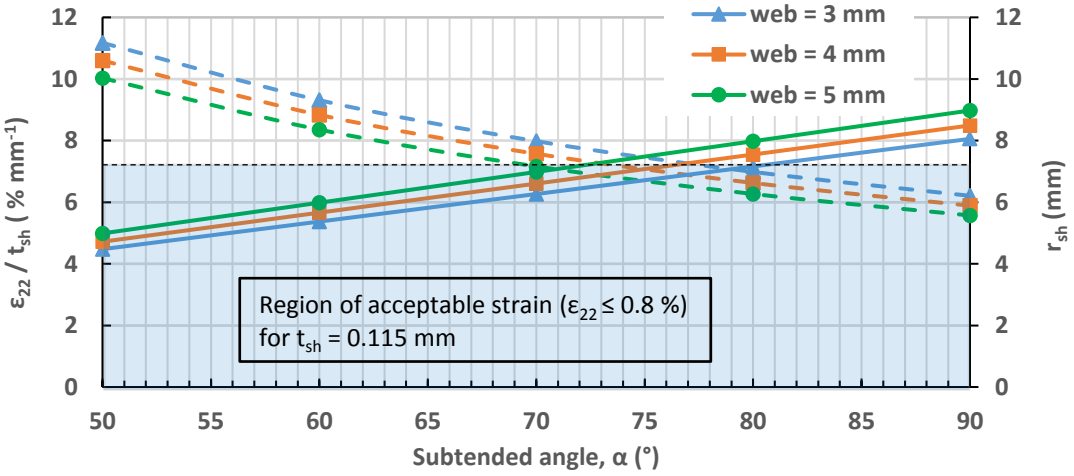

Fig. 4. Transverse strain, ε_{22}, divided by the shell section thickness, t_{sh}, and the radius of curvature of the shell section, r_{sh}, for different combinations of the subtended angles of the cross-section, α, and the web width, w. The solid and dashed lines correspond to ε_{22} and r_{sh}, respectively.

4.1 Fabrication

Traditionally, the omega-shaped shells of CTM booms were fabricated separately and bonded together in a following step. The quality of this process is highly dependent on the bond surface preparation, boom-halves edge alignment, bond line thickness control, and applied pressure. In order to simplify this task and ensure a consistent bonding, DLR has recently developed, as part of the DeorbitSail project, a single step boom manufacturing process.[17)] The boom halves are now co-cured by placing an inner vacuum bag inside the boom cavity and an outer vacuum bag that surrounds the entire tool. The unwanted material surplus, which can be as much as that of the actual boom, is then trimmed to form the edges of the booms.

Following the impetus behind that more cost efficient boom manufacturing technique, a new single step scalable process has been developed following an idea recently shown in 22) for sub-meter class booms. This method consists of, first, fabricating a silicone plug with the shape of the boom using two female (negative) omega-shaped molds. These molds can be manufactured from cheaper materials as they will not be used during the curing process. The easily removable flexible silicone mold will then fill the cavity between boom-halves, acting as an inner male mold and a tool to lay the top half of the boom against. This method eliminates the need for a second tool (top) halving one of the biggest costs incurred during fabrication. An investigation into different silicone materials resulted in the final use of Polytek's Platsil 73-60 liquid silicone rubber giving its high hardness (shore A60), acceptable pour time (45 min), high mixed viscosity (40,000 cP), and almost zero shrinkage during curing for better dimensional reproduction.

Fig. 5 (a) shows the pouring process of the silicone inside two foam molds with a thin Teflon coated fiberglass surface, as well as the final cured shape of the silicone plug. The lightweight foam molds were rattled on a shaker table, to facilitate the release of any air bubbles trapped inside the silicone compound, before being left to cure for 16-20 h at room temperature.

In an effort to reduce the CTE mismatch between the boom material (carbon fiber) and the mold, the initial lower cost polyeurethane foam molds (GP FR4730) of 46.8 ppm/°C were, first, replaced by aluminum molds of 23.4 ppm/°C, and ultimately by carbon foam molds (CFOAM30) of just 5.0 ppm/°C. The CFOAM tool shown in Fig. 5 (b) was fabricated by the Touchstone Research Lab. It has a production surface finish (2.5 mm thick carbon/BMI outer hard shell) that should last over one hundred cure cycles. Reducing the CTE mismatch yielded ever increasing straighter booms, even for non-symmetrical laminates such as ours. The high thermal mass of metallic molds is also not optimal for fabricating very slender booms.

To keep fabrication costs down and aid in the scalability of the process, compatible epoxy resin systems for out-of-autoclave curing, namely PMT-F7 from Patz Materials & Technologies and RS-36 from Tencate, were utilized for the booms. For adhesive bonding of the two boom halves, the aerospace grade Hysol EA 9628 NW in its lightest available form (146 g/m^2) was used. This film adhesive comes with a non-woven nylon mat for better bond line thickness control and cures to a 0.1 ± 0.01 mm thickness. The boom curing cycle adopted has a first 1.25 h long temperature soak at 120 °C to cure the adhesive bond and decrease the viscosity of the resin for adequate fiber impregnation with minimal polymer cross-linking. Then, a second 2 h long temperature soak at 180 °C cures the composite laminate. As recommended by the resin manufacturer, a vacuum pressure ≥ 28 mm Hg is maintained throughout the curing process. However, it was found that relieving vacuum during the final cool-down step to room temperature prevented both ends of the booms from fracturing due to the thermally-induced deformation, particularly when using the metallic molds. Fig. 6 shows some of the steps of the new fabrication process of composite CTM / omega booms.

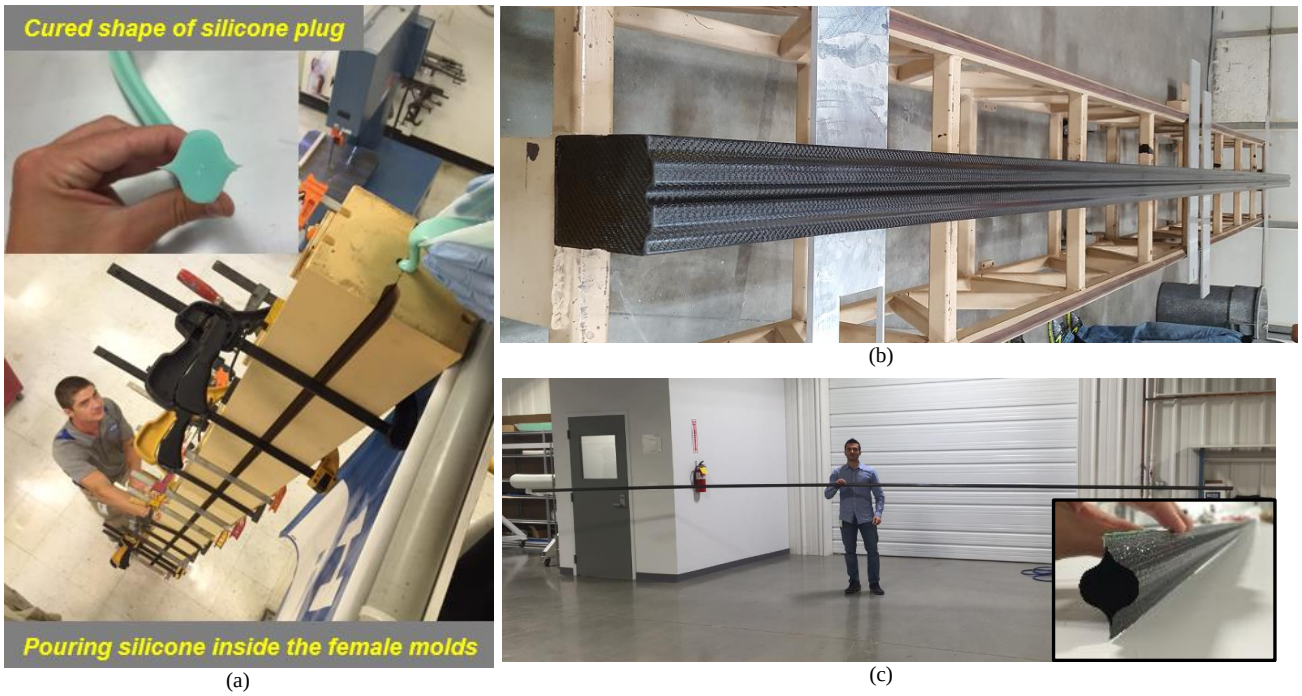

(a) (b) (c)

Fig. 5. (a) Silicone plug mold fabrication process and final shape; (b) two-part 7.3 m carbon mold axially aligned and assembled; (c) 7 m long mini-CTM / omega boom self-supporting under gravity with a close view of its cross-section.

(a) (b) (c) (d)

Fig. 6. Summary of the steps of the boom manufacturing process. (a) Lay down the bottom boom half on top of the female tool using the edge scribe lines for reference. Lay down the silicone plug. Add adhesive strips to the web areas. (b) Lay-down the top boom half pressing it against the silicone plug to conform to its shape. Add a top release film, breather ply and vacuum bag. Apply vacuum and check for leaks. (c) Move the mold into the oven and proceed with the curing cycle. (d) Once processed, release the boom from the female mold and silicone plug. Clean it and sand down the edges.

Several 7 m booms were fabricated with the lower cost aluminum molds for an Engineering Development Unit (EDU) alternative composite solar sail subsystem for NEA Scout. Boom fabrication repeatability and manufacturing errors using these metallic tools were assessed by vertically hanging the as-manufactured booms and measuring their out-of-true in-plane and out-of-plane lateral offsets in the *x* and *y* boom directions, respectively. This gives an idea of the global boom shape (axial curvatures) and could provide a future knock-down factor for boom buckling for imperfect non-straight beam-columns. Table 2 shows the lateral offsets measured by image processing of top view pictures of the tip of the vertically hung booms calibrated with a hung plumb bob for reference and a dot grid paper located on the ground near the boom tip.

Boom #	In-plane offset – *x* (cm)	Out-of-plane offset –*y* (cm)
1	12.5 ± 1	5.0 ± 1
2	10.0 ± 1	1.0 ± 1
3	7.5 ± 1	4.0 ± 1
4	2.5 ± 1	2.5 ± 1

Table 2. Lateral out-of-true deformations measured for the 7 m fabricated with the Aluminum molds.

Deformations in the weak *x*-axis are larger, although, as this direction could be laterally constrained by adjacent tensioned sail quadrants, it could be considered to be less critical than the out-of-plane offsets that could render non-planar sails. The maximum out-of-true straightness offsets found are about 1.8 % and 0. 7 % of the length of the booms in the *x* and *y* directions, respectively. Note that some built-in boom axial curvature may actually be desired for creep mitigation during long-term storage. The recent use of the carbon foam (CFOAM) molds for fabrication of flight-like booms have reduced straightness errors to sub-centimeter, as well as boom-to-boom variability, producing a much more reliable and repeatable manufacturing process.

For the booms fabricated, no appreciable creep-induced axial curvatures were measured after the several months of storage of the testing campaign of the NEA Scout alternative design. However, there was significant flattening of the boom cross-section developed. A maximum 30% loss in boom width (from 23 mm to 16 mm) at the more strained boom root sections was measured. This translates to a theoretical subtended angle, α, loss of 30°, bringing the booms to the lower limit of their working range (see Fig. 3). On the bright side, it seems like this time-dependent deformation has plateaued, which is expected, as material creep deformation is a time-logarithmic phenomenon. A dedicated creep test campaign on material coupons and boom section samples using the time-temperature superposition principle is planned for the near term, in order to better assess the long-term creep behavior of the booms and bound the detrimental effect.

5. Ultra-Thin TRAC Boom

The Triangular Rollable And Collapsible (TRAC) boom was invented by researchers of the US Air Force Research Laboratory (AFRL) a decade ago.[23] The aim was to design a boom architecture with a large cross-section inertia to packaged height ratio. For reference, the TRAC boom has about 10 and 34 times more inertia for the same packaged height and stowed strain than CTM and STEM booms, respectively.[9] The drawback of this boom is its low torsional stiffness. However, the packaging mechanics of the booms require a challenging energy balance between the stored strain energy from pinching together the two flanges and the strain energy from rolling the flat pinched boom around a cylindrical hub. This would otherwise result in the inner boom flange bifurcating from flat to open while in the rolled configuration and thus hindering packaging efficiency. After several iterations of boom laminates, it was determined that the best stacking sequence was to have a balanced laminate with a significant percentage of surface 0° axial unidirectional plies on both sides. However, such axially stiff laminates yielded designs that could not be rolled onto diameters smaller than 18 cm [24], discarding them for CubeSat applications. To allow more compact designs at the expense of mass efficiency, metallic versions of the booms made from stainless steel or Elgiloy alloys were also developed. These versions flew on NanoSail-D2 [25] and LightSail-A [26], respectively, and the Elgiloy one is also currently the baseline solar sail boom for LightSail-B [27] and NEA Scout. [2] However, a recent study presented in 3) raised concerns surrounding the use of unshaded, uncoated metal TRAC booms. Thermally-induced deflections of the booms under direct sunlight exposure may produce a non-controllable solar sail spacecraft that could also collapse under combined thermal/compressive loading. This has led to a major design change of the solar sail for NEA Scout that shifted from a four-quadrant configuration to a single square sheet design, where the sail passively acts as a sun shade for the uncoated Elgiloy TRAC booms. Obviously, the configuration constraint of having to shade the booms continuously would not be feasible for a wide range of other small satellite applications.

The objective of this on-going research is to investigate alternative lightweight composite TRAC boom designs using thin-ply materials that could lead to packaged configurations several times smaller than previously produced, whether or not these can comply with the boom length requirement of NEA Scout. The study presented in 3) concluded that some of the thin-ply CFRP TRAC boom designs proposed herein could exhibit a tenfold decrease in thermally induced curvature and tenfold increase in effective compressive boom strength compared with uncoated Elgiloy designs because of the reduced thermal expansion and induced thermal bowing.

The cross-section geometry adopted aimed at maximizing the moment of area about the *x* and *y* axis for a flattened height of the boom of $h = 45$ *mm*, web width of $w = 6$ *mm*, and the use of a standard tubular mandrel size for fabrication, i.e. 1”, 1.25”, 1.5”,... in diameter. For this, a flange shell radius of r_{sh} = 25.4 mm (2” diameter mandrel size) and a flange subtended angle of

$\alpha = 88°$ was chosen. For such a geometry, the moments of area about the x and y axes are $I_{xx} / t_{sh} = 9870\ mm^3$ and $I_{yy} / t_{sh} = 10567\ mm^3$, respectively, and the torsional constant is $J / t_{sh} = 0.91\ mm^3$. These values were found by numerical integration of every segment of the cross-section shown in Fig. 7 (a). Note that these properties have been divided by the flange thickness, t_{sh}, as this parameter will vary from boom to boom. Fig. 7 shows the computed cross-section of this TRAC boom and a fabricated sample. It can be seen that there is good agreement between the two.

Several TRAC boom samples between 0.3 m and 1.8 m in length and with different stacking sequences of the materials from Table 1 were fabricated in order to assess the performance of the laminates proposed. Table 3 shows some of the most promising laminates fabricated. More laminates have been tested to date but will not be presented herein for brevity.

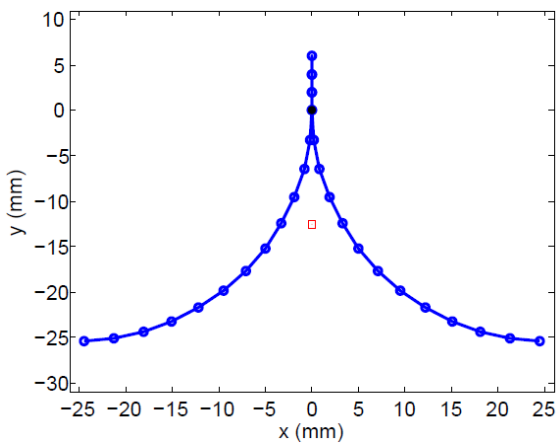

(a)

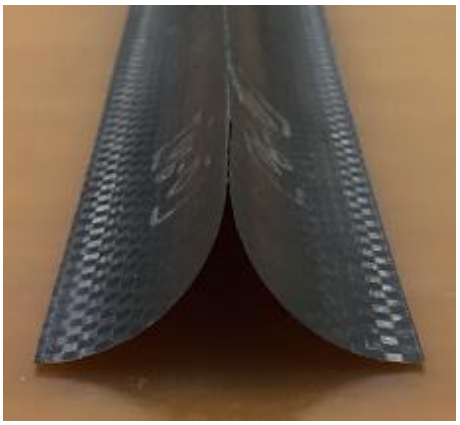

(b)

Fig. 7. (a) Computed ideal optimized TRAC boom cross-section. The red square defines the location of the center of mass and the black circle the start of the web area. The blue dots define the node location of the FEM mesh; (b) Cross-section of a fabricated thin-ply composite TRAC.

Ultra-Thin TRAC_...	Inner Shell Material [outer ply/inner ply]	Outer Shell Material [outer ply /inner ply]	Inner Shell Thick. (mm)	Outer Shell Thick. (mm)	Min. Exp. Wrap Diam. (mm)	Max. Boom Length Allowed† (m)	Inner Shell E_{11} (GPa)	Outer Shell E_{11} (GPa)	Bi-stable
v1	[0-90PW_C]	[0-90PW_C]	0.085	0.085	50	8.74 – 6.74	75.9	75.9	
v2	[0_C/0-90PW_C]	[0_C/0-90PW_C]	0.135	0.135	75	3.49 – 2.87	110.3	110.3	
v3	[0_C/0-90PW_C]	[0_C/45PW_C]	0.135	0.135	65	4.78 – 3.93	110.3	71.7	
v4	[0_C/45PW_C]	[0_C/45PW_C]	0.135	0.135	85	2.01 – 1.66	71.7	71.7	
v5	[0-90PW_C]	[0_C/45PW_{AQ}/0_C]	0.085	0.175	50	6.55 – 5.36	75.9	97.4	
v6	[0-90PW_C]	[0_C/45PW_C/0_C]	0.085	0.180	50	6.46 – 5.30	75.9	101.1	
v7	[0_C/45PW_C/0_C]	[0-90PW_C]	0.180	0.085	80	2.82 – 2.30	101.1	75.9	
v8	[0_C/45PW_{AQ}/0_C]	[0_C/0-90PW_C]	0.175	0.135	65	4.31 – 3.61	97.4	110.3	
v9	[0_C/45PW_{AQ}/0_C]	[0_C/45PW_{AQ}/0_C]	0.175	0.175	140	N/A	97.4	97.4	
v10	[0_G/45PW_{AQ}/0_G]	[0-90PW_C]	0.190	0.085	65	4.72 – 3.89	41.7	75.9	
v11	[0_G/45PW_{AQ}/0_G]	[0_C/45PW_C]	0.190	0.135	75	3.04 – 2.56	41.7	71.7	
v12	[0_G/45PW_C/0_G]	[0_C/0-90PW_C]	0.190	0.135	85	1.75 – 1.48	43.7	110.3	
v13	[0_G/45PW_C/0_G]	[45PW_{AQ}/0_C/45PW_{AQ}]	0.190	0.200	55	4.48 – 3.82	43.7	51.2	
v14	[45PW_{AQ}/0-90PW_C]	[0_C/0-90PW_C]	0.155	0.135	60	5.09 – 4.22	47.7	110.3	
v15	[45PW_C/0_C/45PW_C]	[0-90PW_C]	0.215	0.085	72 (56)*	3.61 – 3.00	51.8	75.9	X
v16	[45PW_C/0_C/45PW_C]	[0_C/45PW_C]	0.215	0.135	79 (56)*	2.40 – 2.04	51.8	71.7	X
v17	[45PW_C/0_C/45PW_C]	[0_G/45BR_C]	0.215	0.16	70 (56)*	3.24 – 2.77	51.8	33.5	X

Table 3. Summary of the most promising laminates for the Ultra-Thin TRAC boom evaluated to date.
C – carbon fiber; AQ – Astroquartz; G – glass fiber, PW – plain weave; BR – braid;
† The length allowed is for two booms co-reeled about the Min. Exp. Wrap Diam. listed for a max. outer coiling diameter of 97 mm. There was a large dispersion on the bond line thickness measurement so, to calculate the total boom thickness, a value of 0.10-0.18 mm should be added. Therefore, the set of boom length values listed correspond to these two extreme cases.
* These are the boom secondary stable coiling diameters. In parenthesis are the inner shell stable coiling diameter alone.

Evaluating the maximum boom length allowed for the TRAC boom designs listed in Table 3, it is clear that the only laminate that would comply with NEA Scout volume requirements is version v1. Possibly, also, v4 and v5, if a slightly thinner bond line thickness can be achieved consistently. Some of the preliminary conclusions that can be drawn from Table 3, which could serve as recommendations or guidelines for the laminate design of ultra-thin TRACs are as follows:

- Designs where the flange thicknesses of the inner and outer shells are significantly different behave distinctively than those where shell thicknesses are similar. This is due to a shift of the neutral axis location when coiling about a hub, from the web center-line towards the thicker shell. For example, v3 can be coiled about a 60 mm diameter hub, whereas v7 only at 80 mm as it is limited by inner shell local buckling rather than fiber fracture or delamination.
- For dissimilar half-boom thickness designs, it is more volume compact to have the inner shell as the thinner one. For example, as shown in Fig. 8, in v6, local buckling of the inner shell is contained within the total thickness of the coiled boom, whereas in v7 the bifurcation translates to a global loss of packing efficiency.
- For samples with similar half-boom thicknesses, it is more volume efficient to have a less stiff outer shell. Compare v3 against v2, which have the same inner shell laminate. However, an inner/outer shell combination that is not stiff enough can result in a loss of compactness as in v4. This is not true for v1 though, which is the thinnest and more compact sample fabricated.
- A single [0-90PW$_C$] ply inner shell is effective towards reducing the minimum coiling diameter regardless of the outer ply stack, though at the expense of overall boom stiffness/strength. Compare the laminates v1, v5 and v6.
- Inner shells with a large lateral bending stiffness when pinched (high E_{11} and t_{sh} combination) prevent inner shell bifurcation but cannot be coiled about small diameters. Nonetheless, if this is chosen, a laterally stiffer outer flange is desired. Compare laminate v7 against v8.
- The inner shell laminate of the form [0_G/45PW/0_G], which has a large strain to failure, can achieve smaller coiling diameters in combination with another flexible laminate outer shell (v13). Also, less stiff outer shells allow a smaller diameter. Compare the v10, v11 and v12 designs.
- The stable coiling diameter of a bi-stable TRAC boom will grow as the lateral bending stiffness of the outer shell increases. Compare the v15, v16 and v17 designs.
- Where possible, all-carbon laminates are preferred over hybrid ones to reduce the boom CTE.

(a) (b)

Fig. 8. (a) Inner shell bifurcation causing global deformation for the v7 laminate; (b) inner shell local buckling contained within the coil for the v6 laminate. The outer diameter of the coil measured at the web and flanges sections are very similar, which indicates a small loss of packaging efficiency.

5.1 Bi-TRAC Boom

Bi-stable versions of the TRAC boom, coined the Bi-TRAC, have been developed for the first time. The mechanics behind achieving bi-stability in TRAC booms are current focus of study. The design approach followed has been to produce a boom with a non-symmetrical construction with respect to its symmetry plane, i.e. dissimilar halves. The inner shell of the boom, that has to coil in an equal-sense way around the drum, is made with a bi-stable laminate, which will bound the natural coiling diameter of the whole boom. The outer shell, that has to coil in a more energetic opposite-sense way, is made with a less stiff mono-stable laminate with a large strain to failure. During boom packaging, the naturally bi-stable half side encloses the mono-stable one at each overlap, having the strain energy of the outer flange well managed, such that bifurcation to the extended state during boom deployment only occurs on the unrestricted outermost wrap of the coil. The boom secondary coiling diameter for a given bi-stable laminate of the inner shell can also be slightly tailored by the axial modulus, E_{11}, of the mono-stable outer shell.

(a) (b)

Fig. 9. (a) Bi-TRAC_v16 in a stable coiled state; (b) Comparison between bi-stable and mono-stable coiled booms. The Bi-TRAC coiled behavior is similar to that of standard bi-stable tape-spring.

The fact that there is a strain energy minimum state in the coiled configuration helps against bifurcation of the inner flange, which normally drives the maximum and minimum wrapped diameters of TRAC booms along with fiber failure. Whether the secondary equilibrium configuration is stable (fully bi-stable booms) or unstable (semi bi-stable booms), improved behavior during packaging and deployment is obtained. For example, a short 0.3 m Bi-TRAC boom coiled can take 6-8 s to self-deploy rather than the few tenths of a second that a standard TRAC of that length would. The main advantage of bi-stable booms is that predictable and controllable deployment dynamics with a less chaotic 3D motion are obtained, as the transition from coiled to deployed states occurs only at a single section of the boom. This "instability" travels spirally along the outer perimeter of the coiled boom steadily unfurling it in sections. The size and complexity of the boom deployment mechanisms involved can thus be reduced when compared to those of traditional mono-stable boom designs, enabling lighter and more compact concepts overall. Fig 9 shows a Bi-TRAC in the coiled configuration, as well as a mono-stable TRAC and a bi-stable tape-spring.

5.2 Fabrication

Fabrication of the TRAC booms also follows a low-cost and scalable process that aims to allow curing the structures without the need of cost and size prohibiting autoclaves. Some of the steps of the manufacturing process are depicted in Fig. 10. The TRAC geometry is achieved by a two-step process. First, each boom-half is fabricated in a cylindrical mandrel to achieve a constant curvature equal to that of the final flange desired. Second, the two individual shell sections are bonded on a common edge to form the final characteristic triangular shape.

To process each cylindrical shell, a similar low-cost fabrication process to that presented in 28) was adopted. This allows very long shells to be manufactured only limited by the length of the mandrel and inner heater. Symmetric laminate shell designs are preferred, as the thermal stresses developed during processing of non-symmetric laminates result in cross-section cupping deformation of the cylindrical shells. For example, to achieve the desired 50 mm diameter radius of curvature on the $[0_C/45PW_C]$ laminates, the shells were formed on a 75 mm diameter mandrel and allowed to cup in. Note that reversing the laminate would result in cupping out to a smaller curvature. This thermal effect prevented fabrication of $[0_C/0\text{-}90PW_C]$ laminate shells longer than 2.5 m, as these tended to crack near each end due to combined thermally-induced cross-section cupping and axial bow deformation. Similarly to what was achieve for the mini-CTM booms, it is possible that relieving pressure during the cool-down step might help solve this problem, though this would be difficult to implement with the heat-shrink wrap technique used herein.

Once each cylindrical shell is fabricated, the process of bonding them is a delicate task. First, each shell is taped down flat to one metallic precision bar aligning its free edge to the precision straight edge of the bar, as shown in Fig. 10 (a). The area for the adhesive bond at the free edge is then masked out with more tape. As shown in Fig. 10 (b), the adhesive is then applied to one of the shells using another straight edge for alignment. The two separate straight edges are ultimately aligned face-to-face to let the two shells come into contact, and taped together at their ends. As shown in Fig. 10 (c), the now coupled part is placed inside the oven with weights on top to provide pressure to the bond line. The curing process for the adhesive (1.25 h at 120° C) is then run. After the bond line is cured, as shown in Fig. 10 (d), the two straight edges are pulled apart by carefully cutting the tape off of one of the shells with a scalpel and applying pressure manually. Finally, as shown in Fig. 10 (e), the second shell is separated from the last straight edge by peeling the remaining line of tape, allowing the boom to spring back into its final triangular shape.

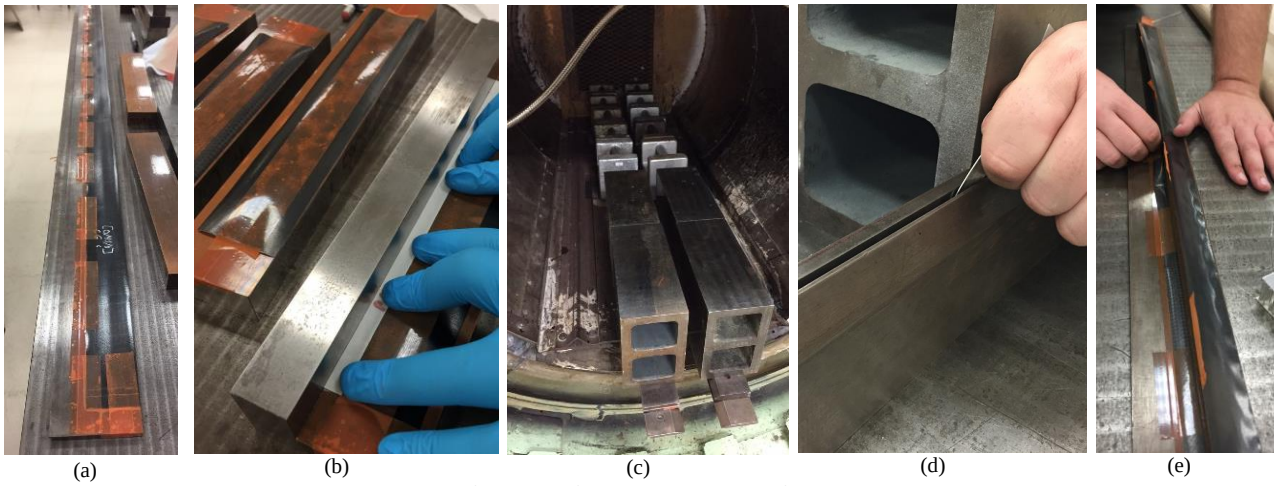

(a) (b) (c) (d) (e)

Fig. 10. Some of the steps of the TRAC boom manufacturing process.

6. SHEARLESS Boom

Previous research gathered in 29) by the author and carried out at the Surrey Space Center in the United Kingdom culminated in several novel rollable boom concepts. One of them had had a biconvex or lenticular () shaped cross-section design. These copper-beryllium (CuBe) metallic booms were first conceived for the CubeSail solar sail mission [30-32], and later redesigned for an ESA funded Gossamer Satellite Deorbiter.[33] Japanese researchers have recently found application of similar shape biconvex booms for deployment of membrane space structure.[34,35] Their main commonality is that the booms are formed by coupling the

edges of two cylindrical shells (i.e. tape-springs) front-to-front by a tightly-fitted outer sheath to form a doubly-symmetrical lenticular/biconvex cross-section. This flexible outer sheath can take multiple forms, from spiral-wound or monolithic plastic tubes to braided sleeves.

The objective of the research presented herein was to improve the performance of the early biconvex boom concepts while keeping their key beneficial features, as well as to try to solve their problematic ones. These new booms are patent pending under the name SHEAth-based Rollable LEnticular-Shaped and low-Stiction (SHEARLESS) composite booms.[36] The main innovation of the SHEARLESS boom comes with the use of composite materials for the inner cylindrical shells to enable lower energy stored configurations, as well as designs that can also be made bi-stable with all the benefits that come with it. The cross-sections of the shells are also optimized for higher moments of area by adopting subtended angles well above the 90º previously produced. Finally, the use of a durable, seamless and low-stiction polymer tube (Teflon™ or fluorinated ethylene propylene (FEP)) as the sheath, enables overall thinner boom designs and reduces creep-induced axial curvature. Fig. 11 shows the key components of the boom in the stored and deployed configuration and compares the cross-section shape with others previously introduced.

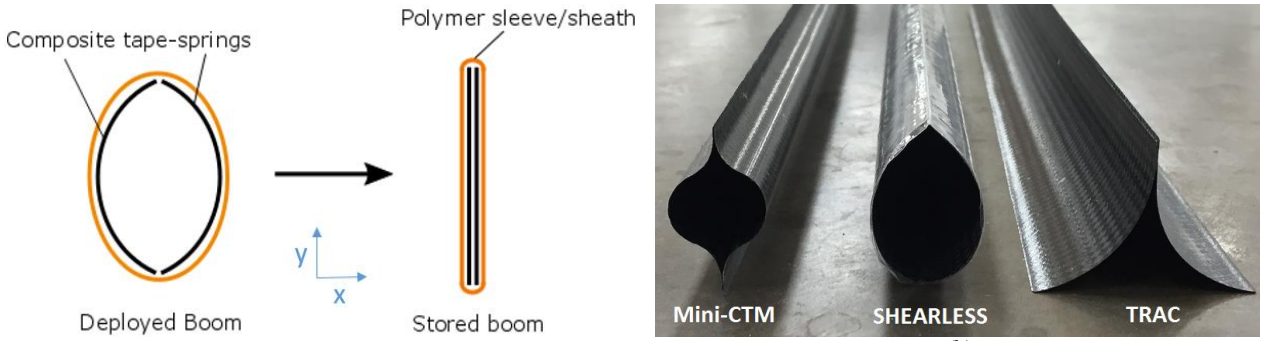

Fig. 11. (a) SHEARLESS boom in the stored and deployed state; (b) comparison of the cross-section shape of the various rollable composite boom concepts presented. All designs have a 45 mm flattened height.

The major challenges of designers of rollable booms formed by bonding or welding two thin-shell walls to increase the structure moment of area per unit of stored/flattened height, as in the TRAC and CTM boom concepts are:

1) The high shear stresses at the joint induced during coiling, which can hinder compactness and boom straightness.
2) The inner shell wall, that undergoes compression loading during coiling, can result in local buckling, which affects packaging efficiency and promotes delamination and crack initiation at the web.
3) The minimum allowable coiling diameter to avoid plastic deformation, that limits the allowable boom length, is limited by the thickness of the web. The material and laminate selection thus becomes critical to meet the conflicting boom requirements of the stored and deployed configurations.
4) The adhesive bonding problems, e.g. durability in space, delamination, long- stowage creep-induced axial curvature.
5) The creation of torsionally stiff booms that will not twist when subjected to imbalanced shear loads, which could induce buckling and collapse.
6) The blossoming phenomenon of the highly energetic boom coil package, which could derive in deployment jamming inside the deployment mechanism and failure.
7) The long-term durability of the boom material in the space environment as coatings for thermal, radiation, atomic oxygen, etc., are difficult to apply to the surfaces of complex-shape booms.
8) Fabrication is somewhat difficult. For example, keeping a precise alignment of the two shell sections during bonding.

The SHEARLESS boom was designed to overcome the challenges listed above while keeping an area moment of inertia per unit of height comparable to state-of-the-art booms. The following benefits are:

1) Storing the boom proceeds in two subsequent steps: flattening of the cross-section and rolling around a hub. During the first step, the edges of the two inner shells are decoupled such that, during the second step, they are allowed to slide axially relative to one another inside the low-friction sheath. Hence, the shear stresses are endured by the flexible sheath rather than the bond line. This promotes more compact and straighter designs.
2) The tight sheath reduces the tendency of the inner shell undergoing compression to buckle locally and affect packaging efficiency.
3) For the same total wall thickness, the minimum allowable coiling diameter is at least halved, allowing more boom length to be packed into the same stowed volume. This enables using high strength and modulus fibers (with less strain to failure) in the laminate, helping bridge the traditionally conflicting requirements of the stored and deployed configurations.
4) The sheath encloses and couples the two inner shells so there are no problematic adhesive bonds in the design. Long-term stowage creep effects are thus reduced.

5) As in CTM designs, the doubly-symmetrical cross-section of the SHEARLESS boom makes the centroid (neutral axis) and the shear center coincident. This eliminates undesired flexural-torsional coupling that can often cause buckling and collapse in torsionally weak slender booms like these.
6) The boom can be designed with a rolled configuration that is in a very low strain energy state, which can even be stable. This helps towards the blossoming phenomenon and increases predictability and reliability of deployment.
7) An outer polymer sheath can be easily coated with environmental protective materials (e.g. thermal coatings or $Si0_2$).
8) Fabrication is simplified by eliminating the bonding process and only having to produce cylindrical composite shells.

The main disadvantage of the SHEARLESS boom and the other biconvex booms is the difficulty in computationally modeling and predicting the structural behavior of the booms given their largely non-linear response. This is a result of the highly contact and friction dependent behavior of the critical coupling effect of the flexible sheath with the inner shells.

As for any cylindrical shell structure, the cross-section of the SHEARLESS boom is defined by only four parameters, which define each tape-spring: the shell thickness, t_{sh}, the flattened height, h, the subtended angle, α, and the radius of the shell, R_{sh}. Of these last three parameters, only two are independent. We assume that, as seen during bending, the two tape-springs are perfectly coupled by the sheath such that the moment of area of the biconvex boom is equal to the sum of the two independent tape-springs about the new centroid. Therefore, the area moment of inertia about the x and y axis can be approximated by:

$$\mathrm{I}_{xx} = R_{sh}^3 t_{sh} [\, \alpha - \sin\, \alpha \,] \,, \tag{6}$$

and

$$\mathrm{I}_{yy} = 2\, R_{sh}^3 t_{sh} \left[\frac{\alpha + \sin\alpha}{2} - \frac{2 - \cos\alpha}{\alpha} + \alpha \left(\frac{\sin(\alpha/2)}{(\alpha/2)} - \cos(\alpha/2) \right)^2 \right], \tag{7}$$

respectively. Fig. 12 shows that, for a given flattened height (45 mm in this case), the way to maximize both area moments of inertia, I_{xx} and I_{yy}, is to sustain a subtended angle of $\alpha = 180^o$ with the smallest radius of curvature possible ($R_{sh} = h / \alpha$). This would yield a circular cross-section (360º) once both tape-springs are coupled. However, circular-like cross-sections are not easy to flatten and can result in nested and decoupled configurations for the two tape-springs upon recovery of the cross-section. Hence, a good compromise is to work with designs where the subtended angles are $150^o \leq \alpha \leq 165^o$. For reference, a 45 mm tall SHEARLESS boom with a $R = 16$ mm, $\alpha = 161.1^o$ design would be, theoretically, slightly stiffer than a TRAC boom about the x-axis (sail plane), $I_{xx} / t_{sh} = 10153\ mm^3$, and about 22% softer about the y-axis (sail out-of-plane), $I_{yy} / t_{sh} = 8219\ mm^3$. These values should be taken with great caution though, given the ideal assumption considered. They can be thought of as an upper bound limit for bending stiffness and limit load calculations.

Unlike for the bending case, where the two tape-springs are well coupled by the sheath for small deformations, in torsion, the sheath only provides a limited amount of coupling and thus each section can somewhat twist independently. To be conservative, for the case of torsion, the SHEARLESS boom should be considered an open-section structure, such that the calculation of the torsional constant, J, takes the known form:

$$\mathrm{J} = \frac{4}{3} \alpha\, R_{sh}\, t_{sh}^3 \,, \tag{8}$$

considering both shells. Thus, the torsional stiffness is several orders of magnitude smaller than that of a similar size closed-section structure ($\propto R_{sh}^3\, t_{sh}$). In reality, as will be shown in the next section, the friction between each tape-spring edge and between the tape-springs and the tight sheath yields a structure torsionally stiffer than the worst case presented above, that can be considered as a lower bound limit.

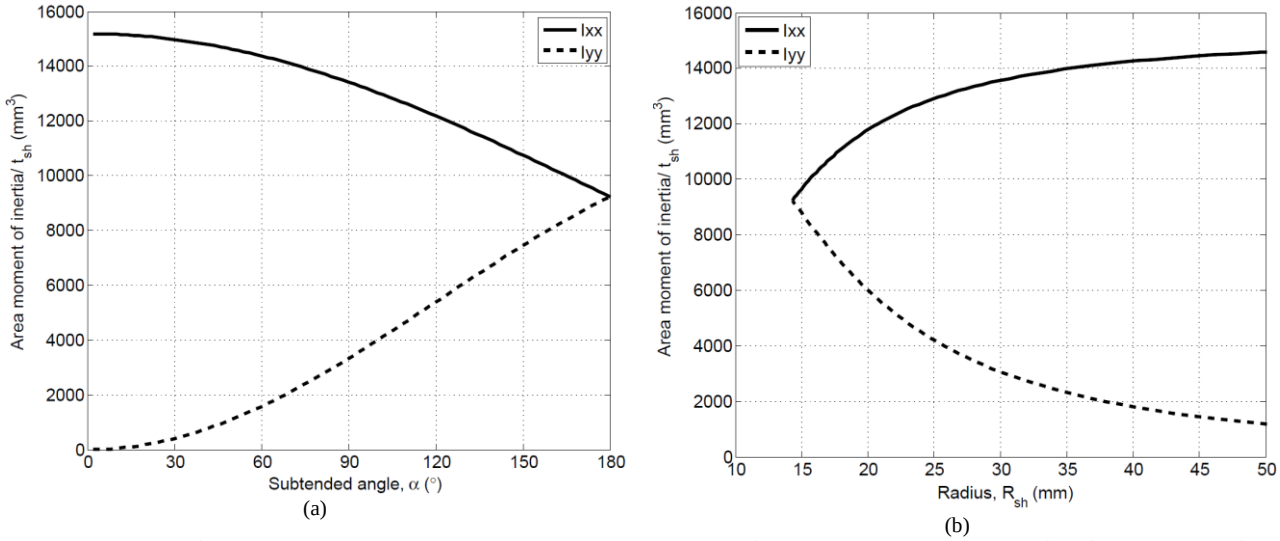

Fig. 12. Area moment of inertia divided by the shell thickness in the two principal axes of the boom cross-section, x and y, for a flattened height of $h = 45$ mm, as a function of the subtended angle (a) and the radius of the cylindrical shells (b).

The flattened inner diameter of the sheath/sleeve, ϕ_{tube}, should be equal to the desired flattened height of the tape-springs, h, plus some clearance, τ. This can be calculated from:

$$\phi_{tube} = \frac{2\,\alpha\,R_{sh}}{\pi} + \tau\,. \tag{8}$$

For tight fits, the clearance should be $\tau = 0.5\ mm$, and for loose fits, $\tau = 1.0\ mm$. For the application at hand, seamless FEP plastic tubes with a diameter of $\phi_{tube} = 29.21\ mm$ were purchased, as it was decided to follow designs with a shell radius of 16 mm and 19 mm with a subtended angle of 161.1° and 135.7°, respectively.

A few of the laminates studied for the Ultra-thin TRAC booms were also used for initial investigations of the SHEARLESS composite booms. It was found that, for the 0.05 ± 0.005 mm wall thick FEP tubes purchased, the thinner laminates could not be used for the preferred tight fit, if significantly long booms were to be produced. The low axial/bending stiffness of the shells when flattened in combination with the large friction build-up after a few meters of tape-spring were coupled, resulted in the shells buckling locally when rolling up the boom and forming sharp corners on the edges that led to fiber damage. Thinner versions could be realized at short lengths of just 1-2 m or at longer lengths with a less desirable loose fit though. For these booms, it is therefore preferred to have stiffer three-ply laminates at the expense of the added thickness and mass.

Table 4 shows the shell laminates studied to date. Note that the packaging efficiency value used in the maximum boom length allowed calculation is 97%, obtained from measuring a few boom samples. In general, the packaging efficiency of this boom is better than that of joined-shell booms. As aforementioned, for the preferred tight fit and the sheath at hand, laminates v4, v5, and v10, which all have a very thin inner shell, could not be realized in the long lengths sought after. Laminates v6 and v9, which have a thicker braided bias ply on the outer shell than v5 and v10, are the only ones that would comply with NEA Scout boom length requirement of 6.85 m. Laminates v1, v2, v3, v7 and v8 are all very promising candidates if a thinner sleeve can be sourced or the outer diameter of the coil can be slightly increased, e.g. to 103 mm for v3.

SHEAR LESS_...	Inner Shell Material [outer ply/inner ply]	Outer Shell Material [outer ply /inner ply]	Inner Shell Thick. (mm)	Outer Shell Thick. (mm)	Min. Exp. Wrap Diam. (mm)	Max. Boom Length Allowed† (m)	Inner Shell E_{11} (GPa)	Outer Shell E_{11} (GPa)	Bi-stable
v1	[0_C/45PW_{AQ}/0_C]	[0_C/45PW_{AQ}/0_C]	0.175	0.175	45	6.12	97.4	97.4	
v2	[45PW_{AQ}/0_C/45PW_{AQ}]	[45PW_{AQ}/0_C/45PW_{AQ}]	0.200	0.200	29	6.41	51.2	51.2	
v3	[45PW_C/0_C/45PW_C]	[45PW_C/0_C/45PW_C]	0.215	0.215	30	6.01	51.8	51.8	
v4	[0-90PW_C]	[45PW_C/0_C/45PW_C]	0.085	0.215	25 (38)*	8.17 (7.41)*	75.9	51.8	X
v5	[45PW_C/0_C]	[45PW_C/0_C/45PW_C]	0.135	0.215	25 (64)*	7.28 (4.40)*	71.7	51.8	X
v6	[45BR_C/0_C]	[45PW_C/0_C/45PW_C]	0.150	0.215	29 (65)*	6.87 (4.16)*	64.1	51.8	X
v7	[45PW_{AQ}/0_C/45PW_{AQ}]	[45PW_C/0_C/45PW_C]	0.200	0.215	30 (71)*	6.18 (3.17)*	51.2	51.8	X
v8	[45PW_{AQ}/0_C/45PW_{AQ}]	[45BR_C/0_C/45BR_C]	0.200	0.255	31 (75)*	5.70 (2.55)*	51.2	45.4	X
v9	[45BR_C/0_C]	[45PW_{AQ}/0_C/45PW_{AQ}]	0.150	0.200	28	7.15	64.1	51.2	
v10	[45PW_C/0_C]	[45PW_C/0_C]	0.135	0.135	25	8.81	71.7	71.7	

Table 4. Laminate properties for the SHEARLESS boom evaluated to date.

C – carbon fiber; AQ – Astroquartz; PW – plain weave; BR – braid;

† The length allowed is for two booms co-reeled about the Min. Exp. Wrap Diam. listed for a max. outer coiling diameter of 97 mm. The sheath adds a max. thickness of 0.11 mm to the total boom thickness. This is what was considered herein.

* The values in parenthesis are the secondary stable coiling diameter and their corresponding max. boom lengths.

The mechanics of the coiling and deployment process of the SHEARLESS boom is current focus of study. The plastic sheath allows the two tape-springs to slide past each other during the coiling/deployment process to account for the difference in wrapping diameter between the two shells as a result of their thickness. This can be seen on Fig. 13. (a), where the outer tape-spring has moved inward of the sleeve during coiling and the inner tape-spring has moved outward of the sleeve creating an offset between the two. This offset is proportional to the thickness and the number of wraps of the coil, which depends on the boom length and initial coiling diameter. During deployment, this offset will reduce until it becomes zero at the end of extension. In the deployed configuration it is preferred that the longitudinal edges of the tape-springs face each other and get coupled throughout the entire length so as to increase the strength and torsional stiffness of the boom structure. The coupled edges are shown in Fig. 13. (b). Nonetheless, as will be presented on the next section, initial tests carried out on sample booms have demonstrated that the torsional stiffness of the deployed structures drop only by 45-65% in the worst case scenario where the tape-spring edges are completely decoupled by shear or nested.

6.1 Bi-SHEARLESS Boom

A secondary stable coiled configuration with a strain energy minimum state can also be induced on SHEARLESS boom designs by engineering the shell laminates. For this, the outer cylindrical shell that coils in an equal-sense way needs to be bi-stable, and the inner shell that wraps in an opposite-sense way needs to be soft and compliant enough to allow the outer shell to prevent its snap-through. An analytical model that will be able to predict secondary stable configurations of the SHEARLESS boom for given laminate designs of the inner and outer shells is being investigated. As with the case of the Bi-TRAC boom, the

secondary stable coiling diameter for a given bi-stable laminate of the outer shell can also be tailored by the axial Young's modulus, E_{11}, of the inner shell. For example, Table 4 shows that for the Bi-SHEARLESS booms fabricated (v4 through v8), that all use an outer shell bi-stable laminate of the form $[\pm 45_C/0_C/\pm 45_C]$, the secondary stable diameter of the boom can almost be doubled (v4 versus v7) as the bending stiffness ($E_{11}I$) of the inner shell grows. In fact, for slightly stiffer inner shell designs, as in v3, the coiled boom is no longer in a stable strain energy minimum configuration.

Fig. 13 (c) exemplifies how the secondary stable diameter of the coil grows when you couple by a sheath a bi-stable tape-springs (28 mm) with a mono-stable tape-spring to form a Bi-SHEARLESS boom (65 mm). Another way to tailor the secondary stable diameter of the coil for a fixed outer to inner shell axial modulus ratio (E_{11o}/E_{11i}) is by changing cross-section design to increase/decrease the moments of area (I_{xx} and I_{yy}). Fig. 13 (d) shows that for the same v4 laminate the boom natural coiling diameter grows from 38 mm, for the R_{sh} = *16 mm* and α = *161.1°* design shown in Table 3, to 75 mm, for the much shallower shell cross-section design depicted with R_{sh} =*25.5 mm and* α = *101.1°*. Note that there will also be a design limit at which shallower cross-sections will cease to yield bi-stable biconvex booms.

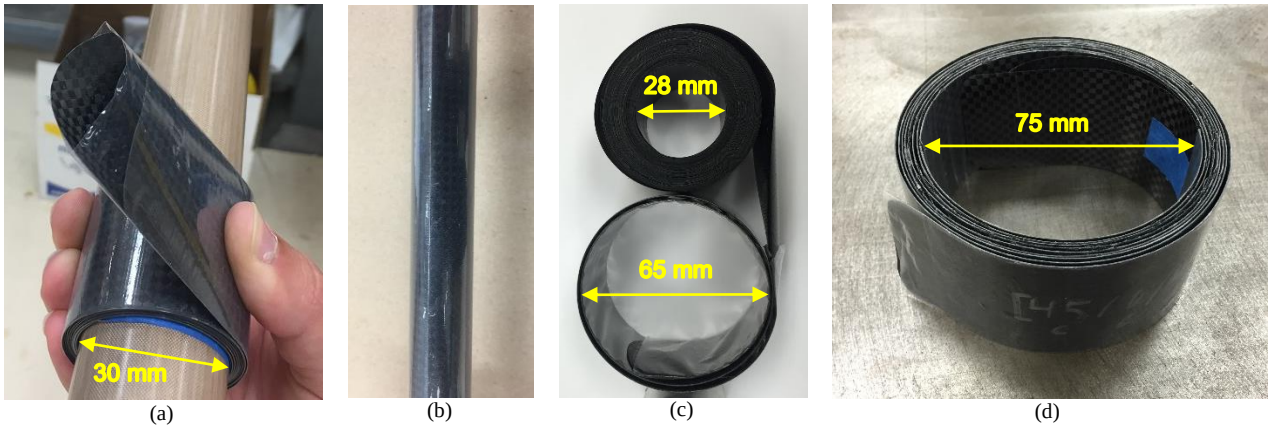

(a) (b) (c) (d)

Fig. 13. (a) SHEARLESS_v3 boom wrapped, showing the relative offset between tape-springs; (b) coupled edges of the tape-springs in the deployed configuration; (c) bi-stable tape-spring (top) used as the outer shell of the Bi-SHEARLESS_v6 boom (bottom), showing the size difference in stable coiling diameter; (d) coiled Bi-SHEARLESS_v4 boom with a shallow cross-section design (α = 101.1°).

6.2 Fabrication

One of the advantages of the SHEARLESS boom concept is that it is very simple to fabricate and does not require dedicated molds or large autoclaves/ovens, which drive the costs up. The SHEARLESS boom is fabricated by, first, independently manufacturing the two tape-springs and, later on, coupling them together with the sheath. As for the case of the TRAC boom cylindrical halves, each shell was fabricated following the low-cost and scalable process presented in [28-29], that makes use of a tubular mandrel heated by an internal heating element and heat-shrink polyester wrap tape that applies pressure to the parts.

The FEP plastic tubular sheath was sized accordingly to the boom dimensions and purchased in a flattened roll form from American Durafilm Co. This guarantees that the two permanent creases required are already perfectly straight, skipping the tedious task of having to crease un-flattened plastic tubes that could result in twisted booms if not done properly. It is recommended that the shells are passed inside the sheath one at a time. Once the first one is completely in, the radius of the second shell should be decreased by hand so as to nest this shell inside the first one. This reduces the friction build-up, as more sections of tape-spring are in, and avoids damaging the shell edges. Finally, once both shells are completely inside the sheath, flattening of the cross-section and subsequent recovery should commence from one end of the boom onwards, coupling the shell edges one boom section at a time until completion.

7. Boom Structural Characterization Tests

In order to gain insight into the mechanical properties of the various new composite booms introduced and to validate finite element models (FEM), a series of purposely designed boom structural characterization test methods were developed. Performance tests with such lightweight slender structures under gravity are always challenging and can lead to errors, and thus where possible, the gravity force was off-loaded or its effects were reduced by the test orientation/configuration adopted.

7.1 Torsion Tests

Torsion tests were carried out with the aim of measuring the torsional stiffness, *GJ*, of the booms as well as calibrate the boom FEM, in particular that for the SHEARLESS boom that relies heavily on empirical data. Fig. 14 (a) shows a top view picture of the torsion test setup. Each boom end was fixed to a three-dimensional (3D) printed plastic fitting that had a slot of the boom cross-section, as shown on the close-up view image. For the test, the boom was clamped vertically downwards from the top end fitting that had square facets. The cylindrical end fitting at the bottom, which was used as a torque wheel, had two Kevlar strings wrapped around that were each in line with a load cell. Each of the load cells was fixed to a metal bar that could travel parallel to the other one on linear rails. As linear displacement increased, the Kevlar strings provided a pure torsional moment to the boom. Tension on the strings, which was measured by the load cells, and the fixed moment arm captured the applied moment.

A camera pointing downwards from the top was used to document the rotation of the bottom end fitting. The relative twist angle at each step measured was found by superimposing two consecutive photographs. Angular rotations of up to 25° and 180° for the stiffer and softer booms, respectively, were normally achieved.

Fig. 14 (b) shows the torsional stiffness measured on all the boom types tested. As expected, the Mini-CTM booms tested, that are the only closed-section structures, outperformed the rest of the open-section booms. The two-ply Mini-CTMs are an order of magnitude stiffer in torsion than their one-ply counterparts, which in turn are an order of magnitude stiffer than the "semi" open-section SHEARLESS booms. TRAC booms of similar thickness are about half as stiff of the thicker three-ply SHEARLESS booms tested, but the thinner 1-ply versions are an order of magnitude smaller. As torsional stiffness grows with the cube of the thickness it is anticipated that three-ply carbon TRAC booms would be equally stiff, although, as was shown in Table 2, these are not optimal for small satellite applications.

A test, where the three-ply SHEARLESS boom had both edges completely decoupled demonstrated that, if this worse case ever manifested, a performance drop in torsion of 45-65% could occur for the boom studied. Both the cases of decoupled edges by shear or by nesting one shell inside the other were tested, giving similar results. Another test, where the plastic sheath was completely removed from the boom, revealed a further order of magnitude decrease in torsional stiffness. This is similar to the result obtained for a single tape-spring of the same three-ply laminate construction.

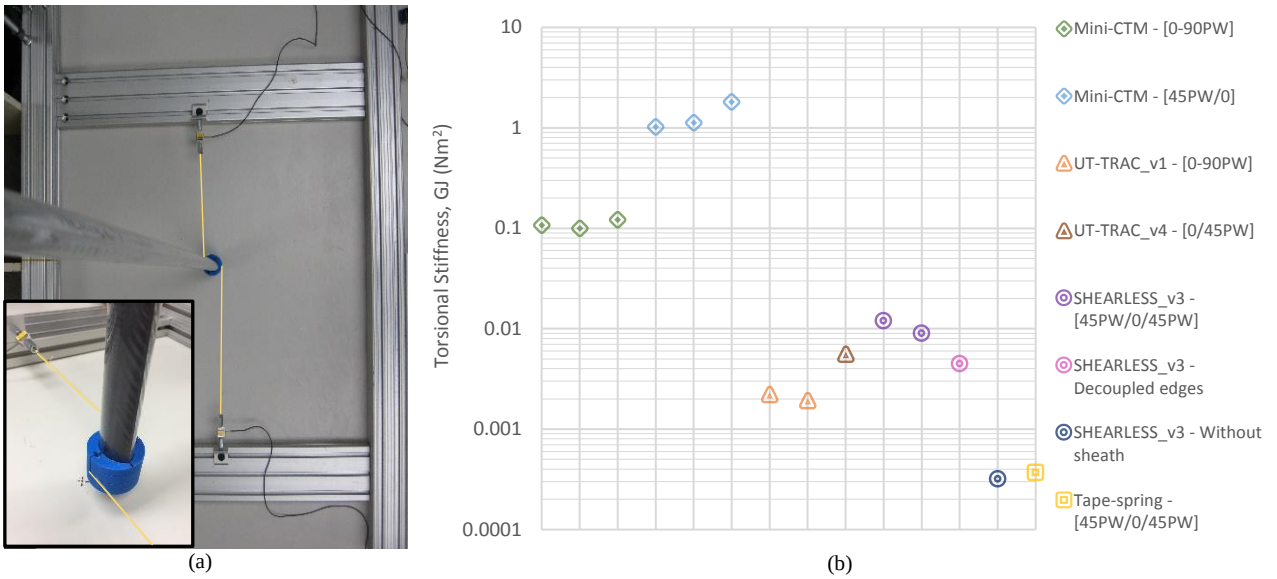

(a) (b)

Fig. 14. (a) Boom torsion test setup; (b) torsional stiffness chart for the various composite boom concepts tested.

7.2 Axial-compressive loading buckling tests

Axial buckling tests with gravity off-loading and under flight-like boundary conditions were also carried out. The purpose was to develop a test setup that could provide realistic boundary conditions for testing long slender structures, as well as to determine the maximum permitted load on some of the half scale (3.25-3.60 m) boom samples fabricated that have potential for being used on NEA Scout or similar solar sail missions.

The booms were tested in a horizontal configuration suspended from a purposely developed whiffle tree as shown on Fig. 15 (a). The beams of the whiffle tree are carbon fiber square tubing and Kevlar strings were used to connect them. The system enables large deflections of the booms during loading without imposing unwanted reactions on the structure. With the amount of tree stages used, free rotations about the mid-point of the boom are allowed, such as for second-order buckling modes. The off-loading masses were placed on two buckets that were hung from the whiffle tree. The masses and off-loading point locations were calculated for the bending moment at the boom root to be zero. Prior to fixing the root, the boom was left free floating to check that the boom remained leveled horizontally, which indicated proper off-loading.

The boom roots were fixed to plastic printed drums that represented plausible future designs of the hubs, which will enable complete or partial recovery of the boom cross-section at the end of deployment. Two fixed lateral constraints, that represented fixed exit rollers of a future deployer design, provided lateral support 5 cm from the boom end. This is in line with some CubeSat-based boom deployer concepts.[33] Fig. 15 (b) shows the root boundary condition adopted for one of the Mini-CTM booms tested.

Sail tension loading on the boom was mimicked by using a Kevlar string that connected the tip of the boom to a reel behind the root that was cranked to apply tension. The string passed through a fixed hole on a metal plate at the boom root section, which represented a load boundary condition of a column with an eccentric load through a fixed point. The location of this fixed point was chosen to best represent the non-symmetric design of a twin-spool/hub square solar sail, such as NEA Scout. The load lines that connect the tip of opposite booms of the sail create a lateral in-plane eccentricity. In this case of 2 cm eccentricity to the right of two booms and 3 cm to the left (here negative) of the other pair of booms. Also, as shown in Fig. 15 (b), the vertical out-of-plane offset (6.8 cm) of the sail plane with respect to the boom plane was captured. An additional in-plane eccentricity of -8 cm was adopted as well to assess the sensitivity of the booms to large asymmetric in-plane loads. As represented on

Fig. 15 (c) left, the Kevlar string, that represents the load line, had a force sensor in series that measured the load applied to the boom.

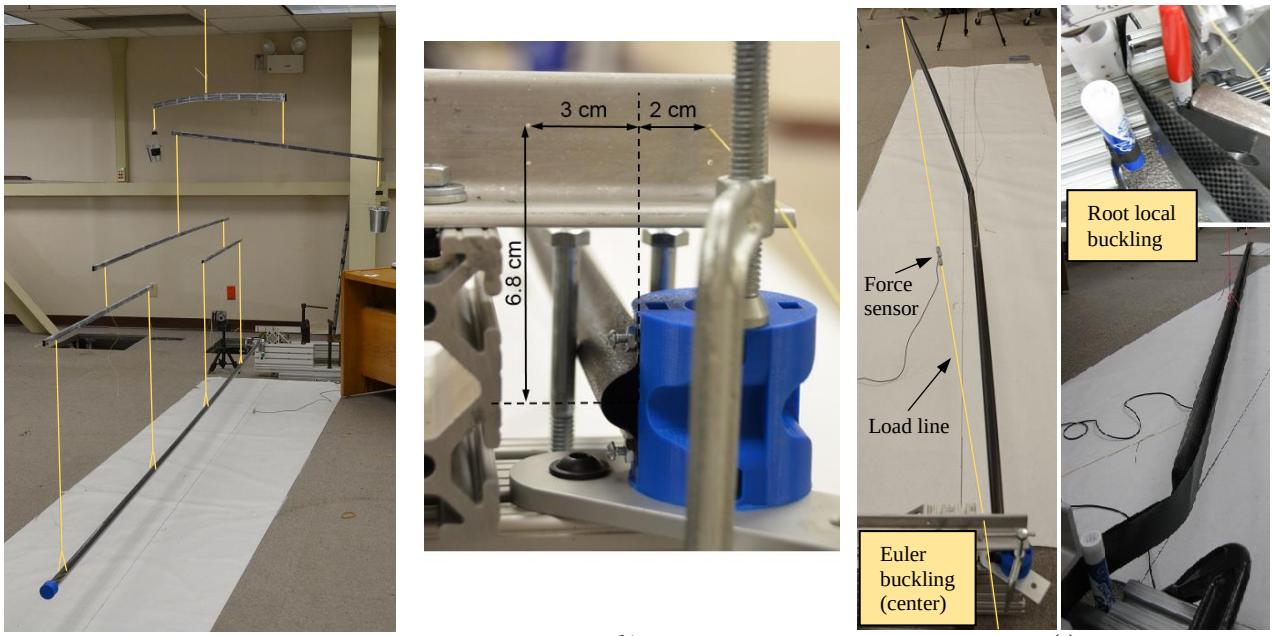

(a) (b) (c)

Fig. 15. (a) SHEARLESS_v3 boom gravity off-loaded from a whiffle tree; (b) Root boundary condition for a Mini-CTM boom tested, showing the hole locations that determine the fixed, load application eccentricity; (c) Euler buckling mode with failure at the boom center for a Mini-CTM with a -3 cm lateral load eccentricity (left), and local buckling failure at the boom root for a UT-TRAC_v1 boom with a +2 cm lateral load eccentricity (right).

Table 5 shows the test matrix followed and the results for all the booms tested. Every boom was tested at least three times in each configuration. The mean peak load values reported all have a low standard deviation. Both Mini-CTM booms and the SHEARLESS boom failed at the center of the boom in a first-order Euler buckling mode. The typical loading graph showed a large plateau near the peak load, which represents a stable post-buckled state with large in-plane lateral deflections, before the onset of local buckling at the center of the boom and subsequent collapse. The full-scale (7 m class) two-ply Mini-CTM booms and the SHEARLESS_v3 boom are expected to have limit loads above the 3 N required for NEA Scout. Longer two-ply Mini-CTMs could potentially perform better for large asymmetric tensioning load cases as collapse of the shorter tested piece is initiated at the root implying that the typical Euler buckling mode, which should be the failure mode of longer booms, would be even higher. The ultralight Mini-CTM could perform well on smaller size sails. For example a 5 m, one-ply [0-90PW] Mini-CTM should have an acceptable buckling load of 3 N, and thus could potentially be used on 50 m^2 solar sails.

Boom	Load lateral IP eccentricity (cm)	Buckling Mode	Length, L (m)	Avg. Peak Load, P_{cr} (N)	P_{cr} scaled to 7 m as: $L^2/49$ (N)
Mini-CTM [45PW/0]	2	Euler	3.27	19.46	4.26
	-3	Euler	3.27	16.38	3.58
	-8	Root	3.27	10.19	N/A
Mini-CTM [0-90PW]	2	Euler	3.50	6.00	1.50
	-3	Euler	3.50	6.23	1.56
	-8	Root	3.50	1.81	N/A
SHEARLESS_v3	2	Euler	3.58	13.44	3.52
	-3	Euler	3.58	11.86	3.10
	-8	Euler	3.58	7.57	1.98
UT-TRAC_v1	2	Root	3.50	1.61	N/A
	-3	Root	3.50	1.34	N/A

Table 5. Axial compressive-loading buckling test results for the various booms tested. The peak load is considered the limit load achieved.

The results of the Ultra-thin TRAC boom are somewhat misleading. This boom was tested with the current NEA Scout drum design, which is for a smaller height boom (35 mm). This means that the flanges of the boom at the root were not allowed to flare out as much as one would like, decreasing the moment of area. This is evident by the root failure mode suffered, which is shown in Fig. 15 (c) right. This test needs to be redone with an updated drum design, which would allow a much stiffer root section, in order to promote a stiffer Euler type buckling mode like that seen on the rest of the booms. The loading graphs of root failure tests showed pointed curves, where the peak load followed immediate loss of load carrying capacity of the booms

and sudden collapse. Hence, achieving this unstable post-buckled state should be avoided by design. As a final note, there may be more risk associated with boom strength during deployment than during operations, where the root is much weaker before full deployment. Hence, deployment testing with sail extension and final tensioning should be the next step to fully validate a boom choice for a particular solar sail design.

8. Conclusions

It has been showcased that, for small satellites components, and in particular for CubeSats, many of the top-level system requirements for the deployable structure can all be flowed down to a material, thickness and cross-section design selection for the supporting booms, all of which are interrelated. Several rollable composite boom concepts have been presented to comply with the stringent mass, volume and structural requirements of an 85 m^2 solar sail housed on a 6U CubeSat, while others will enable similar sail designs on other small satellite platforms. Some of the booms are miniaturized and/or lighter versions of previous concepts, which have been optimized with the use of thin-ply materials, while others are new designs. These booms are also applicable to a wide range of other applications for small satellites. For each boom concept, the low-cost fabrication process was shown, which has been developed to enable out-of-autoclave manufacturing of very long slender structures of a few tens of meters. Larger cross-section designs of these rollable booms would also be applicable to much larger sails in the 1000-1500 m^2 area range that could still be housed on small satellites, i.e. ESPA-class platforms.

The Mini-CTM boom with a [45PW/0] laminate construction satisfies all the NEA Scout requirements listed and has the best structural performance of all the booms tested. The torsional stiffness is several orders of magnitude larger than the rest, and the limit loads for axial compression are also the highest obtained. Manufacturing boom-to-boom variability and straightness errors, measured as *x-y* lateral out-of-true deformations, of the order of 10 cm and 5 cm in the in-plane and out-of-plane boom/sail directions obtained with the initial aluminum molds have been corrected with the use of the low CTE carbon foam tools, producing near-perfectly straight booms consistently. For the booms fabricated, no appreciable creep-induced axial curvature was observed after several months of storage. However, there was significant flattening of the cross-section measured as a maximum of 30% loss in boom width, which halves the critical in-plane buckling load of the booms, bringing them close to the loading threshold established. A future dedicated creep test campaign will assess and bound the long-term stowage deformation and relaxation effects of this time-logarithmic phenomenon, which should plateau at a certain time. These high performance rollable booms are currently being utilized by NASA on an advanced solar sail propulsion system for future small spacecraft.[37)]

Designing an ultra-thin composite TRAC boom to comply with NEA Scout requirements proved to be very difficult. Only designs with the thinner-most laminates studied would fit, but, as seen, will likely not comply with structural requirements. Further axial loading tests on longer booms with optimized hub designs will need to be carried out to assess their suitability for such large sails. The minimum wrap diameter of the booms was, in general, limited by inner shell bifurcation during coiling and not laminate strain failure. It is thus expected that the use of higher modulus carbon fiber unidirectional materials of a similar low thickness could improve the boom load carrying capacity for some of the thinner laminates without affecting the stowed volume. Also, decreasing the total web thickness, by achieving more consistent thinner bond-line thicknesses or dropping inside plies on that region, would minimize the minimum wrap diameter, and thus allow more boom length to be housed within an available volume.

The SHEARLESS composite boom was presented to solve some of the challenges of joined-shell boom concepts. It shows great potential for finding a middle ground between the higher performance and more scalable CTM boom, the larger moment of area per unit of stowed height TRAC boom, and the more accessible and lower cost production tape-springs or STEMs. To achieve long booms with the preferred tight sheaths, the thicker three-ply laminates studied were found to give better results at the expense of added mass and volume. For these, it was found that the critical torsional stiffness would be increased ten-fold and two-fold when compared to one or two-ply TRACs, respectively, which are competing advanced open-section boom concepts that allow similar boom lengths to be packaged in the same volume. Also, the axial-compressive strength was lower, but of the same order, as an equivalent closed-section boom concept, namely the two-ply [45PW/0] Mini-CTM.

Secondary stable coiled configurations with a strain energy minimum state were induced for the first time on TRAC booms, as well as on the new SHEARLESS boom introduced. For this, the cylindrical shell that coils in an equal-sense way around the hub needs have a bi-stable laminate, and the other mono-stable shell needs to be soft and compliant enough to allow the bi-stable shell to still develop a strain energy dwell around the coiled configuration, preventing the snap-through or bifurcation to the extended state. The natural coiling diameter of these two-shell bi-stable booms can be tailored by the bending stiffness (E_{11} I) ratio of the inner and outer shells. The less stiff the mono-stable shell is, the closest the natural coiling diameter of the complete boom would be to that of the bi-stable shell coiled alone. In fact, less compliant and stiffer mono-stable shells can prevent the boom from attaining a stable, minimum energy secondary state in the coiled configuration. Shallower shell cross-sections (low subtended angles) would also cease to produce two-shell bi-stable booms. The scalability of these bi-stable composite booms could potentially be increased following the design approach investigated in 28).

Acknowledgements

This research is financially supported by NASA's Advanced Exploration System (AES) program under the future exploration projects portfolio and NASA's Space Technology Mission Directorate (STMD) under a Game Changing Development Program (GCDP) project to advance deployable shell-based composite booms. Initial seedling funding was obtained by a NASA LaRC's Independent Research and Development (IRAD) activity for solar sail technology development managed by W. Keats Wilkie.

Help from past NASA interns, Charles White and Matthew Lee, as well as from the composite fabrication technicians, Jacob Tury and Kevin McLain, is gratefully acknowledged.

References

1) Murphey, T.W., et al., *High Strain Composites*, 2nd AIAA Spacecraft Structures Conference, Kissimmee, Florida, 2015, AIAA 2015-0942.
2) McNutt, L., et al., *Near-Earth Asteroid Scout*, AIAA SPACE 2014 Conference and Exhibition, San Diego, California, 2014, AIAA 2014-4435.
3) Stolhman, O., Loper, E. R., *Thermal Deformation of Very Slender Triangular Rollable and Collapsible Booms*,
4) Rimrott, F.P.J., *Storable Tubular Extendible Member…A Unique Machine Element*, Machine Design, 37, No. 28, 156-165, 1965.
5) Yee, J.C.H., Soykasap, O., Pellegrino, S., *Carbon Fiber Reinforced Plastic Tape Springs*, 45th AIAA/ASME/ASCE/AHS/ASC Structures, Structural Dynamics and Materials Conference, Palm Springs, California, 2004, AIAA 2004-1819.
6) Fernandez, J.M., Lappas, V.J., Daton-Lovett, A.J., *Completely Stripped Solar Sail Concept Using Bi-stable Reeled Composite Booms*, Acta Astronautica, Vol. 69 (1-2), 78-85, 2011.
7) Jeon, S.K., Murphey, T.W., *Design and Analysis of a Meter-class CubeSat Booom with a Motor-less Deployment By Bi-stable Tape Springs*, 52nd AIAA/ASME/ASCE/AHS/ASC Structures, Structural Dynamics and Materials Conference, Denver, Colorado, 2011, AIAA 2011-1731.
8) Fernandez, J.M., et al., *Deployment Mechanisms of a Gossamer Satellite Deorbiter*, 15th European Space Mechanisms & Tribology Symposium, Noordwijk, The Netherlands, 2013.
9) Roybal, F.A., Banik, J.A., Murphey, T.W., *Development of an Elastically Deployable Boom for Tensioned Planar Structures*, 48th AIAA/ASME/ASCE/AHS/ASC Structures, Structural Dynamics and Materials Conference, Honolulu, Hawaii, 2007, AIAA 2007-1838.
10) Herbeck, L., et al., *Development and Test of Deployable Ultra-Lightweight CFRP-Booms for a Solar Sail*, European Conference on Spacecraft Structures, Materials, and Mechanical Testing, Noordwijk, The Netherlands, 2000.
11) Rennie, B.B., *New Closed Tubular Extendible Boom*, 2nd Aerospace Mechanisms Symposium, ed: Herzl, G.G., JPL, TM 33-355, 163-170, 1967.
12) Crouch, D.S., *Mars Viking Surface Sampler Subsystem*, 25th Conference on Remote Systems Technology, 1977.
13) Armstrong H.H., Johnson R.R., *Organic & Metal Matrix Composites for Spacecraft Applications*, SAMPE Quarterly, 1978.
14) Aguirre-Martinez, M.A., Bureo-Dacal, R., Del Campo, F., Fuentes, M., *The CTM family of Masts and the CTM Engineering Model*, 3rd European Space Mechanisms & Tribology Symposium, Madrid, Spain, 1987.
15) Aguirre-Martinez, M.A., et al., *The Development of a Continuous Manufacturing Method for a Deployable Satellite Mast in CFRP*, British Plastics Congress, 107-110, 1986.
16) Geppert, U., et al., *The 3-step DLR-ESA Gossamer Road to Solar Sailing*, Advances in Space Research, Vol. 48, 1695-1701, 2011.
17) Hillebrandt, M., et al., *The Boom Design of the De-Orbit Sail Satellite*, 13th European Conference on Spacecraft Structures, Materials and Environmental Testing, Braunschweig, Germany, 2014 (ESA SP-727, June 2014).
18) Hakkak, F., Khoddam, S., *On Calculation of Preliminary Design Parameters for Lenticular Booms*, Proceedings of the Institution of Mechanical Engineers, Part G: Journal of Aerospace Engineering, Vol. 221, No. 3, 377-384, 2007.
19) Murphy, D., Murphey, T.W., Gierow, P., *Scalable Solar-Sail Subsystem Design Concept*, AIAA Journal of Spacecraft and Rockets, Vol. 40, No. 4, 539-547, 2003.
20) Greschik, G., et al., *A Rule of Thumb for the Suspension of Film Sheets without Catenaries*, 44th AIAA/ASME/ASCE/AHS/ASC Structures, Structural Dynamics and Materials Conference, Norfolk, Virginia, 2003, AIAA 2003-1907.
21) Fernandez, J.M., et al., *Design and Development of a Gossamer Sail System for Deorbiting in Low Earth Orbit*, Acta Astronautica, Vol. 103, 204-225, 2014.
22) West, S., et al., *Design and Testing of Deployable Carbon Fiber Booms for CubeSat Non-Gossamer Applications*, 56th AIAA/ASCE/AHS/ASC Structures, Structural Dynamics and Materials Conference, Kissimmee, Florida, 2015, AIAA 2015-0206.
23) Murphey, T.W., Banik, J., *Triangular Rollable And Collapsible Boom*, U.S. Patent 7895795 B1, filed in October 2007 and published in March 2011.
24) Banik, J.A., Murphey, T.W., *Performance Validation of the Triangular Rollable And Collapsible Mast*, 24th Annual AIAA/USU Conference on Small Satellites, Logan, Utah, 2010, SSC10-II-1.
25) Alhorn, D., et al., *NanoSail-D: The Small Satellite That Could*, 25th Annual AIAA/USU Conference on Small Satellites, Logan, Utah, 2011, SSC11-VI-1.
26) Biddy, C., Svitek, T., *LightSail-1 Solar Sail Design and Qualification*, 41st Aerospace Mechanisms Symposium, Pasadena, California, 2012.
27) Ridenoure, R., et al., *LightSail Program Status: One Down, One to Go*, 29th Annual AIAA/USU Conference on Small Satellites, Logan, Utah, 2015, SSC15-V-3.
28) Fernandez, J.M., et al., *Bistable Over the Whole Length (BOWL) CFRP Booms for Solar Sails*, Advances in Solar Sailing (ed: MacDonald, M.), 609-628, Springer Praxis Books, Springer-Verlag Berlin Heidelberg, 2014.
29) Fernandez, J.M., *Low-Cost Gossamer Sail Systems for Solar Sailing and Spacecraft Deorbiting Applications*, Ph.D Thesis, Surrey Space Center, University of Surrey, UK, 2014.
30) Adeli, N.S., *Deployment System for the CubeSail nano-Solar Sail Mission*, 24th Annual AIAA/USU Conference on Small Satellites, Logan, Utah, 2010, SSC10-VIII-3.
31) Fernandez et al., *CubeSail: A Low-Cost Nano-Solar Sail for Space Debris Reduction in LEO*, 1st IAA Conference on University Satellite Missions, Rome, Italy, 27-29 January 2011.
32) Lappas et al., *CubeSail: A Low-Cost CubeSat Based Solar Sail Demonstration Mission*, Advances in Space Research, Vol. 48, Issue 11, 1890-1901, 2011.
33) Fernandez et al., *Deployment Mechanisms of a Gossamer Satellite Deorbiter*, 15th European Space Mechanisms and Tribology Symposium, Noordwijk, The Netherlands, 2013.
34) Natori, M.C., et al, *Deployable Membrane Structures with Rolled-up Booms and Their Deployment Characteristics*, 54th AIAA/ASCE/AHS/ASC Structures, Structural Dynamics and Materials Conference, Boston, Massachusetts, 2013, AIAA 2013-1596.
35) Katsumata, N., et al., *Deployment Characteristics of Braided Coated Bi-Convex Tape and Bi-SMA Convex Tape Booms for Deployable Membrane Structures*, Journal of Mechanics Engineering and Automation, Vol. 4, 52-62, 2014.
36) Fernandez, J.M., *Sheath-Based Rollable Lenticular-Shaped and Low-Stiction Composite Boom*, U.S. Patent Application 15/245,515 filed on 24 August 2016.
37) Fernandez, J.M., et al., *NASA's Advanced Solar Sail Propulsion System for Low-cost Deep Space Exploration and Science Missions that uses High Performance Rollable Composite Booms*, 4th International Symposium on Solar Sailing, Kyoto, Japan, 2017.